Experimental Study of the ³⁸S Excited Level and Decay Scheme

C. R. Hoffman, 1, * R. Lubna, 2, 3 E. L. Rubino, 4, † S. L. Tabor, 4 K. Auranen, 1, ‡ P. C. Bender, 5 C. Campbell, 6 J. Chen, 1 M. Gott, 1, § J. P. Greene, 1 D. E. M. Hoff, 5, † T. Huang, 1, ¶ H. Iwasaki, 3 F. Kondev, 1 T. Lauritsen, 1 J. Li, 3, ¶ J. Saiz, 7 C. Santamaria, 6, ¶ D. Seweryniak, 1 S. Stolz, 1 T. L. Tang, 1, ** G. L. Wilson, 8, 1 J. Wu, 1, †† and S. Zhu¹, ‡‡ 1 Physics Division, Argonne National Laboratory, 9700 S. Cass Ave., Argonne, IL 60439, USA 2 TRIUMF, 4004 Wesbrook Mall, Vancouver, British Columbia V6T 2A3, Canada 3 Facility for Rare Isotope Beams, Michigan State University, East Lansing, Michigan 48824, USA 4 Department of Physics, Florida State University, Tallahassee, Florida 32306, USA 5 Department of Physics and Applied Physics, University of Massachusetts Lowell, Lowell, Massachusetts 01854, USA 6 Nuclear Science Division, Lawrence Berkeley National Laboratory, Berkeley, California 94720, USA 7 Department of Physics, University of York, Heslington, York YO10 5DD, United Kingdom 8 Department of Physics and Astronomy, Louisiana State University, Baton Rouge, Louisiana 70803, USA

(Dated: October 7, 2022)

I. INTRODUCTION & BACKGROUND

First discovered in 1958 [1], ³⁸S is comprised of sixteen protons (Z = 16) and twenty-two neutrons (N = 22) $[T_z = 3]$. Its positioning on the chart of the nuclides is such that two valence neutrons reside outside of the traditional N=20 shell closure defined by the $\nu 1s0d$ - $_{20}$ 0f1p shell gap while valence protons fill two-thirds of the $\pi 1s0d$ shell including all of the $\pi 0d_{5/2}$ orbital. The ground state and low-lying structure in ³⁸S lends itself to a competition between the single-particle aspects of the $\pi 1s0d$ and $\nu 0f1p$ orbitals and more coherent or collec-25 tive forces. The near degeneracy of two sets of $\Delta J=2$ orbitals for instance, provide a solid foundation for the development of quadrupole correlations. Higher-lying excited levels in ³⁸S are not surprisingly expected to be additionally influenced by various particle-hole cross-shell 30 excitations in addition to the aforementioned effects. It is these same properties which underlie the low-lying and ground state behavior in the neutron-rich Si and S iso-

The $^{38}\mathrm{S}$ ground state has a lifetime of $\mathrm{T}_{1/2}=$ 35 170(1) min and β^- decays with a branch of 100% [2]. A number of excited levels have been observed below 7 MeV based on data collected from β -delayed γ -ray spectroscopy [3], two-particle transfer reactions - some that incorporated γ -ray detection [4–8], and in-beam γ -ray spectroscopy measurements utilizing deep inelastic reactions [9–12] or intermediate energy fragmentation [13].

* calem.hoffman@gmail.com

10

A summary of the level energies and J^{π} values was presented in Fig. 6.46 of Ref. [12]. Firm spin-parity (J^{π}) assignments were established only for the yrast even- J_{5} levels through $J^{\pi}=4^{+}$ and the 2_{2}^{+} level at 2.806 MeV. A probable candidate for the yrast 6_{1}^{+} level was first observed in the work of Ref. [9]. Candidates for possible negative parity (intruder) states starting at around 3.5 MeV up through \sim 6 MeV were also identified, primarily in the (t,p) or β decay works [3, 6]. Additional spectroscopic information with respect to the excited levels in 38 S, such as transitions strengths [B(E2) values] for a number of levels, and the ratio of the multipole matrix elements (M_n/M_p) and the g factor for the $2_1^+ \rightarrow 0_1^+$ transition, have been extracted from in-beam Coulomb excitation or inelastic scattering data [14–20].

The energies of the established yrast levels in ³⁸S have been well described by considering valence protons within the 1s0d shell and valence neutrons with the 0f1p shell. Reproduction of the energy levels by the weak-coupling model prescription of Bansal and French [21] within this single-particle space, i.e. $^{36}S\otimes^{42}Ca$, was shown in Fig. 4 of Ref. [6]. The goodness of the weak-coupling model confirms there is little change in the 1s0d proton interactions between ³⁶S-³⁸S and similarly for the two neutrons in the 0f1p shell between the $^{42}\text{Ca-}^{38}\text{S}$ isotones. Unsurprisingly, a number of effective interactions derived within this model space have also been successful in reproducing the observed level energies and the even-Jyrast states in particular. For instance, there are the results of the SDPF interactions of Refs. [22–24] shown in Fig. 4 of Refs. [6] and [7], respectively. Other interactions, more recently developed for the region such as the SDPF-MU [25], the sdpf-nr [26], and sdpf-u [27] interactions have each also been successful in describing the lowlying level energies (see Fig. 4 of Ref. [13] and Fig. 6.46 of Ref. [11]). In addition, they have also shown promise in describing the quadrupole collectivity in ³⁸S via general agreement with experimental B(E2) strengths [14, 20] and the measured $0^+ \rightarrow 2_1^+$ g factor [17].

The present work describes the first investigation of ³⁸S excited-state levels and their decay properties via population in a fusion-evaporation reaction. In doing so, a

 $^{^\}dagger$ Present Address: Lawrence Livermore National Laboratory, Livermore, CA 94550.

[‡] Present Address: Department of Physics, University of Jy-vaskyla, P.O. Box 35, FI-40014 University of Jyvaskyla, Finland.

 $[\]S$ Present Address: Oak Ridge National Laboratory, Oak Ridge, Tennessee 37831, USA.

[¶] Present Address:

^{**} Present Address: Department of Physics, Florida State University, Tallahassee, Florida 32306, USA

^{††} Present Address: Brookhaven National Laboratory, National Nuclear Data Center, Upton, New York 11973, USA.

^{‡‡} Deceased

significant number of new excited levels and transitions were determined from the in-beam γ -ray data, uniquely selected following ³⁸S recoil identification. In particular, the yrast even-J levels have been extended to $8^{(+)}$ and a number of higher-J candidates obtained. γ -ray multipolarities have been deduced for some transitions based on γ -ray yields and were used to assign or suggest J-values where possible. The resulting level and decay scheme are discussed in terms of simple symmetry arguments, the trends in the region, and compared directly with shell-model calculations including the FSU cross-shell interaction [28].

II. EXPERIMENTAL DETAILS

Excited states in ³⁸S were populated in the $^{18}\mathrm{O}(^{22}\mathrm{Ne},2p)$ fusion evaporation reaction at \sim 45 MeV. A 48.5 MeV ²²Ne⁶⁺ primary beam at an intensity of 100 30 particle-nano-Amperes was provided by the Argonne Tandem Linear Accelerator System (ATLAS) Facility located at Argonne National Laboratory. The ¹⁸O targets were prepared by electrodeposition. A 1 mL aliquot of 99% ¹⁸O H₂O was added to the deposition chamber seated on top of a $\sim 1.1 \text{ mg/cm}^2$ Ta foil. Electrodeposition was performed using a platinum cathode and the Ta foil as the anode, which was held at a constant +100 V DC for approximately 5 hours. As the ¹⁸O diffused into the Ta foil, the surface passivated resulting in the cur-110 rent dropping from several hundred μA to tens of μA . Mass gain and alpha loss measurements indicated a few hundred $\mu g/cm^2$ of ¹⁸O were diffused into one side of the $\sim 1.1 \text{ mg/cm}^2$ Ta foil. The Ta foil was arranged so that the $^{18}\tilde{\mathrm{O}}$ material resided on the downstream target 115 side allowing the best possible release of heavy-ion recoils. The beam energy was chosen to take into account the energy loss through $\sim 1/2$ of the Ta foil and assumed that the ¹⁸O material was evenly distributed in the latter half of the foil. No degradation in the amount or $_{120}$ distribution of the $^{18}{\rm O}$ material was observed over the duration of the run (~ 6 days).

Prompt γ -ray transitions emanating from the reaction were detected in the Gamma-Ray Energy Tracking Array (GRETINA) [29]. GRETINA consisted of 12 HPGe modules that were positioned to cover polar-angles between $70 < \theta < 170^{\circ}$ relative to the beam direction. Relative energy-dependent detection efficiencies and energyresponse calibrations were carried out with standard γ ray sources of ¹⁵²Eu and ⁵⁶Co. The data collected was 130 processed in an add-back mode whereby γ -ray interactions that occurred within 10 cm of each other were energy summed. Both the source and in-beam γ -ray data was processed the same way. The position information from the largest-energy interaction were used to define the outgoing γ -ray angle for Doppler reconstruction. Similarly, the timestamp from largest-energy interaction was used as the timestamp for that event and used for relative-timing coincidences. An average recoil

velocity of $\beta=0.003375(15)/c$ was uniquely determined for the ³⁸S recoils from a fit of the known 1293-keV and 1534-keV γ -ray energies as a function of polar angle. An energy resolution of $\sim 0.5\%$ FWHM was measured for the 1293-keV γ -ray in ³⁸S.

The Fragment Mass Analayzer (FMA) [30] provided 145 selection capabilities for recoiling ³⁸S ions via energyto-charge, E/q, and mass-to-charge, A/q, ratios. The magnetic and electric elements of the FMA were optimized for the transmission of ³⁸S⁸⁺ at 18.7 MeV, i.e., A/q = 38/8 = 4.75 and $E/q = 18.7/8 \approx 2.338$. Mov-150 able slits in the dispersive direction were used at the FMA focal plane to remove nearby A/q ambiguities and to reduce the intensity of scattered un-reacted primary beam. Both dispersive (horizontal) and non-dispersive (vertical) position information was collected event-byevent at the FMA focal plane by a parallel-grid avalanche counter (PGAC) filled with isobutane gas to a pressure of 3 Torr. Timing signals to both trigger data collection and for use in the event-by-event time-of-flight reconstruction originated from the PGAC anode signal. An ionization chamber (IC) having a segmented-anode readout consisting of two 5 cm long sections followed by a 20 cm long section, was positioned directly behind the PGAC. The IC was operated with isobutane gas at a pressure of 8 Torr which ensured the stopping of all recoils of interest within its volume. The recoil-ion energy information was recorded independently for each of the three sections, E_i (i = 1 - 3).

All of the data was collected by a digital data acquisition system which sampled the input analog signals at a frequency of 100 MHz. The valid condition to activate data collection was a relative time-coincidence of $< 1\mu s$ between the timestamp of the PGAC anode a timestamp from GRETINA when the γ -ray multiplicity condition of $\gamma_{Mult} > 0$ was met. Typical data-collection rates were on the order of ~ 5 kHz and were set by the upper rate limits in the FMA focal plane detectors.

III. EXPERIMENTAL & ANALYSIS METHODS

A. ³⁸S recoil selection

There are a number of two-proton evaporation analyses prior to this work which involved the selection and identification of isotopes of interest by the FMA [31–33]. Each of those leveraged some combination of the following quantities to extract the events of interest: i) the relative times between prompt γ -rays and the PGAC $(T_{\gamma-PGAC})$ to provide suppression of random coincidences, ii) the individual or summed ionization chamber energy information (E_i, E_{ij}, E_{ijk}) to identify the element (Z) of interest, iii), the dispersive position of the recoil at the FMA focal plane (x) to define A/q, and iv) the combined (total) ion chamber energy, E_{123} , with the recoil time-of-flight $(T_{\gamma-PGAC})$ to distinguish A through the classical mass relation, $m \sim E_{123}T_{\gamma-PGAC}^2$. In the present work, the

beam energy and extra target thickness due to the Ta foil matrix, resulted in relatively low energies for the recoiling $^{38}{\rm S}$ ions ($\lesssim 20$ MeV). The consequence was a less than optimal identification of $^{38}{\rm S}$ recoils based on a series of manual selections or gates applied to the quantities listed above. For instance, as viewed in Figs. 1(a) and (c), gates applied to the ionization chamber energies included large overlaps the with the neighboring isobar $^{38}{\rm Cl}$. In addition, the dispersive position $x \propto A/q$ plot in Fig. 1(e) identifies an overlap between the A/q=38/8 recoils of interest with a nearby A/q=33/7 ambiguity belonging to $^{33}{\rm P}^{7+}$.

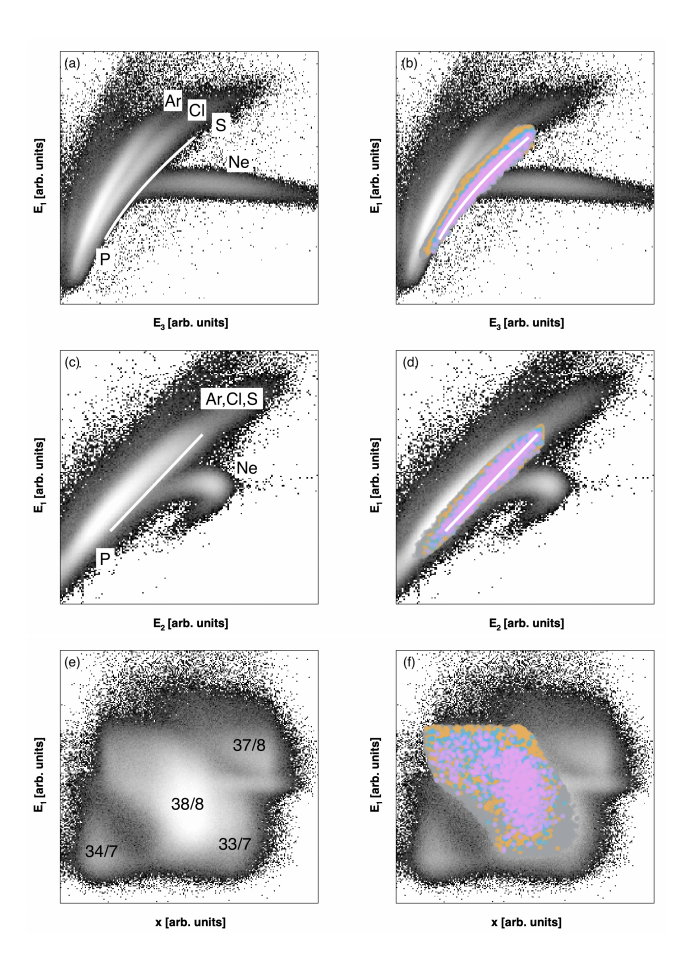


FIG. 1. The energy of the first ion chamber section (E_1) plotted against the energy of the second section (E_2) (a)-(b), the third section (E_3) (c)-(d), and the dispersive position at $_{250}$ the FMA focal plane (x) in (e)-(f). The time-coincidence gate $|\Delta T_{\gamma-PGAC}| < 200$ ns was applied to the grey-scale histograms which are the same across each row. Element (Z) labels in (a) and (c) identify the general regions of interest, while the white line identifies the central region covered by 38 S recoils. The labels in (e) correspond to A/q values. The overlaid spectra in (b), (d), and (f) include data which define the manual cuts (grey points) and from the various model output values, $k_{ml} > 0.25$ (yellow), 0.60 (blue), and 0.81 (pink), as defined in Fig. 4 (see text for additional details).

1. Application of a fully-connected feed-forward neural network model

To improve upon the selection of ³⁸S recoils over the application of manual gating alone, a fully-connected feed-forward neural network (NN) model was developed and implemented. This is the first application of such a model to be used for assisting with recoil selection at the FMA. The power of trainable NN models for various classifications scenarios is now wide-spread and impactful across nuclear science research, see for example Ref. [34] and references therein. In the present work, we developed and trained through supervision an NN model with the ability to process our event data in a goal oriented One-Vs-All mode. In this mode, the ³⁸S recoil data is meant to be distinguished, or classified, against all other types of recoil data. Types of data not belonging to ³⁸S recoils included other fusion-evaporation reaction channels resulting in ³⁸Cl and ³³P recoils, random data originating from the ¹⁸¹Ta lattice and scattered primary beam, and Compton-scattering background data. The framework of the NN model was designed to output a single value, k_{ml} , ranging from 0-1, for each data input into the model. In one sense, k_{ml} is representative of the degree or likelyhood to which the model has found the corresponding input data to be to classified as ³⁸S (approaching a value 230 of 1) or not (approaching towards 0). An individual γ -ray energy, after the add-back procedures described in Section II, was used to define a unique set of input data to the NN model. For each γ ray, eleven experimental values were associated with it, defining the input size of the first 235 NN model layer. For example, an event with a γ -ray multiplicity of 5, $M_{\gamma} = 5$, was considered as five independent sets of data inputs into the model. The input values included the individual and summing permutations of the ion chamber energies $(E_1, E_2, E_3, E_{12}, E_{13}, E_{23}, E_{123})$, the 240 FMA focal plane dispersive plane position information (x), the relative recoil time-of-flight from the target to the FMA focal plane $(T_{\gamma-PGAC})$, the calculated mass $(m \sim E_{13}T_{\gamma-PGAC}^2)$, and the γ -ray multiplicity (M_{γ}) of the complete event to which the individual γ -ray belonged. The number of input parameters could have been reduced due to redundancies and correlations, for example, the parameters used to generate m were all included independently. However, the calculated values were already readily available and the number of inputs were relatively small. As is standard practice, each input value range was independently normalized to span from 0-1 to reduce the possibility of any biases appearing throughout the NN model training.

The framework of the NN model itself was standard and considered to be shallow. It consisted of three total layers, an input layer with dimensions (x11,x40), a hidden layer (x40,x20), and an output layer (x20,x1). Each corresponding layer was linearly- and fully-connected with the previous one. The rectified linear unit (Relu) and Parametric Relu (PRelu) functions [35] were applied to the input and hidden layers, respectively. A Sigmoid

activation function was applied to the output layer. A dropout function [36] was active between the input and hidden layers with a 20% probability for zeroing any in-265 dividual neuron within that layer. In total, there were 1322 trainable parameters: 480 for the input layer, 820+1 for the hidden layer plus PRelu function, and 21 for the output layer. The NN model was trained under supervision through gradient descent and back-propagation using the Binary Cross Entropy Loss (BCELoss) function and Adam optimizer [37] with a learning rate of $1e^{-2}$ and exponential decay rate values of $\beta_1 = 0.9$ and $\beta_2 = 0.999$ on the first and second moment estimates, respectively. In addition to exploring the number and sizes of neu-275 tron layers, the drop-out fraction, and learning rate parameters, other so-called hyper-parameters explored such as the batch size and the epoch number. No hyperparameter showed significant impact on the quality of the training and outputs. The largest sensitivity to the 280 overall quality and performance of the NN model came from the type, size, and scope (in terms of the manual gating) of the training-data used for the supervised training.

2. Manual data reduction and defining the training data

The NN model was able to be trained, under supervision, by labeling a sub-set of data based on γ -ray energy. This was possible because there are known transitions for both the recoil of interest, 38 S [9–11, 13], as well as for 38 Cl [38], 33 P [39], and 181 Ta [2]. Fig. 2 and Table I show 290 and list, respectively, the γ -ray energies used for labeling the NN training data. Input values that were associated with a $^{38}{
m S}$ γ -ray energy $\pm 1-2$ keV were labeled with a value $\equiv 1$. Other types of data with the requisite γ -ray energies $\pm 1 - 2$ keV were similarly labeled as $\equiv 0$. Note that: i) not all γ -rays with the appropriate energies were labeled and used for training (additional details below), and ii) γ -ray spectra inherently contain backgrounds from various sources as shown in Fig. 2. Due to the latter, generation of a "clean" data set for training 300 was not possible. As a result, there were large contributions to mislabeled events, ranging anywhere from $\sim 10\%$ to > 50% for each of the γ -ray energies included in the training data set.

A manual reduction of the data was used to pre-define 335 a region of events for inclusion into the NN model for training data selection as well as for the analysis which followed. The manual selections aided in further reducing random coincidences, background events, and hence, mislabeled training data, over a timing-coincidence require- 340 ment alone. Also, the manual gates were aimed at removing an initial overwhelming number of events from 38 Ar and 38 Cl that were not interfering with the cleanliness of the 38 S spectra. Therefore, in addition to a requirement that events have a time relation of $|\Delta T_{\gamma-PGAC}| < 200$ ns, 345 selections were also derived from the E_1 - E_2 , E_1 - E_3 , and E_1 - E_2 2-dimensional spectra as show in Fig. 1. The en-

TABLE I. Energies and numbers of known γ -ray transitions that were included in the manual gating, selected for labeling, and used as NN model training data.

	$E_{\gamma} \; (\text{keV})$	# labeled	label	Refs.
	384	8600		
^{38}S	1293	18460	$\equiv 1$	[9-11, 13]
	1535	11940		
	171	20610		
³⁸ Cl	292	21110		
	638	10210		
	1190	7260	- 0	[oe]
	2044	4790	$\equiv 0$	[38]
	2275	5880		
	2972	6530		
	3142	5630		
	1432	14840		
³³ P	1848	21250	$\equiv 0$	[39]
	2379	12900		
$^{181}\mathrm{Ta}$	136	25910	$\equiv 0$	[2]

ergy selections represented by the grey data points in Figs. 1(b) and (d) were able to remove all events linked to the ³⁸Ar isobar, as well as a large portion of the the ³⁸Cl recoil events. The gates also reduced the number of random γ -ray events caused by scattered ²²Ne primary beam. The selection region shown in Fig. 1(f) on E_1 -x removed most of the mass ambiguities. However, the the $A/q \approx 33/7$ region was purposefully not removed so as to ensure enough ³³P events remained for labeling and inclusion in the NN model training. In total, $\sim 5.5e^6$ γ -rays remained after the manual selections (Fig. 2). Included within those data were the $\sim 195 \mathrm{k}$ events labeled for training, ~ 39 k 38 S, ~ 82 k 38 Cl, ~ 49 k 33 P, and ~ 26 k Ta (Table I and 2). In order to provide better balance to the training data, the labeling of the $^{38}\mathrm{Cl}$ and $^{181}\mathrm{Ta}$ data was down-sampled by a factor of 4 each.

3. NN model training & output

The training of the NN model specifically refers to the adjustment and eventual optimization of the 1322 model parameters described above. The supervised training of the NN model, whereby we utilized our labeled data, was completed by cycling through the labeled training data 200 times (200 epochs). The loss calculations and backward propagation were calculated and carried out in batches of 500 pieces of data. Changes in the epoch and batch size parameters were explored but did not significantly alter the model performance. Throughout the training procedure, the model output value k_{ml} was rounded to its nearest integer (0 or 1) prior to the loss calculation. Various iterations into the type and scope of the manual data selection, as described above, were ex-

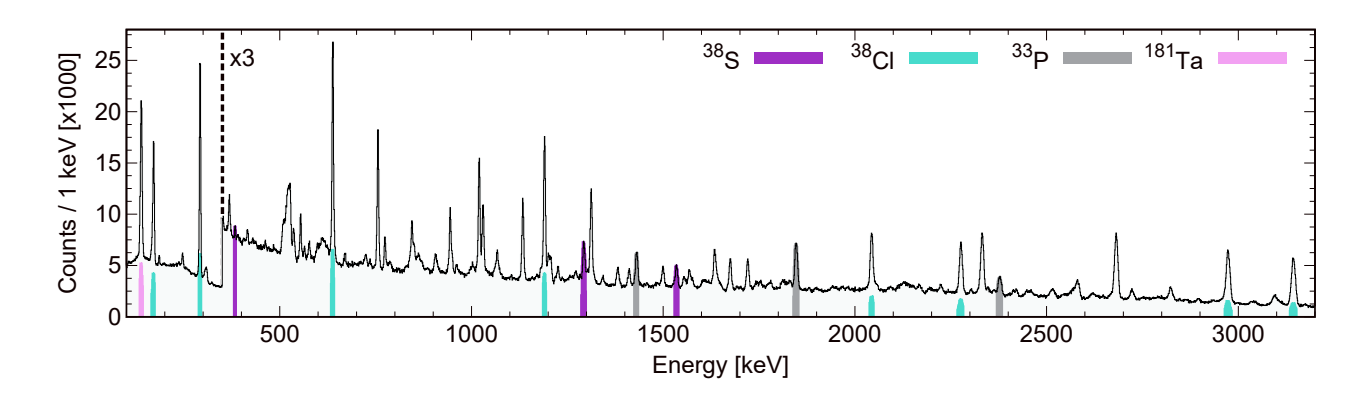


FIG. 2. The total spectrum of γ rays encompassed within the composite manual gating regions. The labeled events used for the NN model training data set are distinguished by the colored regions.

plored in order to reach the adopted parameters for the NN model. Metrics typically used in defining the goodness of trained machine-learning models were not crucial in the determination of the applicability of the model in this case. This is in part due to the known mislabeling of a large fraction of training events which would lead to ambiguities in most standard metrics.

To first order, the distribution and trends of the k_{ml} values provided straight-forward visual feedback of the NN model's ability to separate ³⁸S data from the rest. This can be visualized through the evolution of the k_{ml} values for the training data throughout the actual train-360 ing process (Fig. 3). In Figs. 3(a - d) the distributions for k_{ml} are shown at the conclusion of different epoch 400 numbers (1, 5, 10, and 100) for the labeled ³⁸S training data (purple lines) as well as the sum of all other labeled training data (black lines). As expected, after a_{55} a single pass through the data (epochs = 1) both types of labeled data have similar distributions. As the epoch number grows, the ^{38}S data starts trending towards $\equiv 1$ faster than the other data types, and even after only 10 epochs, a peak forms for the ³⁸S data above $k_{ml} > 0.5$. $_{370}$ By the completion of 100 epochs, the distributions are different and a sub-set of data, peaking towards $k_{ml} = 1$ identifies the ³⁸S data within the model. Fig. 4 also shows the breakdown of the individually labeled components for the training data k_{ml} distributions with the fully-trained model (epochs = 200). One sees that little evolves between epochs 100 - 200. Also, the behavior of each non-³⁸S type is similar.

Beyond the distribution of the k_{ml} values alone, the integrated number of counts between some starting value of k_{ml} up to $k_{ml} = 1$ was calculated throughout the training. The behavior of the fractional counts remaining out of the total (given in percent) are displayed in Figs. 3(e - h). The trends mimic those of the k_{ml} distributions as expected and highlight the unique persistence of the 38 S counts while increasing the lower limit on the integration. The entirety of the data encompassed within the

manual-cut regions (Figs. 1 and Figs. 2), not just the labeled data, was similarly evaluated by the fully-trained NN model. The distribution of the output k_{ml} values is shown in Fig. 4. The complete data set and the labeled training data were used to define the k_{ml} values applied in the final analysis. Contaminant γ -ray yields showed the most dramatic reduction in counts when $k_{ml} \gtrsim 0.25$, i.e. integration of counts between $0.25 \le k_{ml} \le 1$. The ³⁸S yields varied only slightly through this transition point. In addition, the ³⁸S recoils remained nearly constant over $0.25 \lesssim k_{ml} \lesssim 0.8$, while contaminant yields continued to reduce. Above $k_{ml} \gtrsim 0.8$ all events showed diminishing yields.

Finally, the validity of each trained model was also evaluated by quality of the γ -ray singles spectra that they could generate. Specifically, the labeled training data was used to check ratio between the summed areas of known transitions in $^{38}\mathrm{S}$ [9–11, 13] compared to the relative summed areas of the known transitions in $^{38}\mathrm{Cl}$ [38] and $^{33}\mathrm{P}$ [39]. For consistency, the comparison was made at a k_{ml} value in which the area of the $^{38}\mathrm{S}$ 1293-keV transition was $\equiv 5000$ counts. The γ -ray spectra from each NN model training were also visually inspected and overlaid with each other to qualify background and random-event suppression. The resulting spectra are presented in Section IV.

B. Additional prompt γ -ray information

In addition to a γ -ray singles spectrum for a specific k_{ml} value, a recoil- γ - γ coincidence matrix was generated from data which had γ -ray multiplicities $M_{\gamma} > 1$. To be included in the matrix, a pair of γ rays must have had a relative timing relation of < 200 ns and both have been within the accepted k_{ml} cut range. The cut range $k_{ml} > 0.25$ was primarily used in the analysis due to its compromise between cleanliness and statistics. In cases

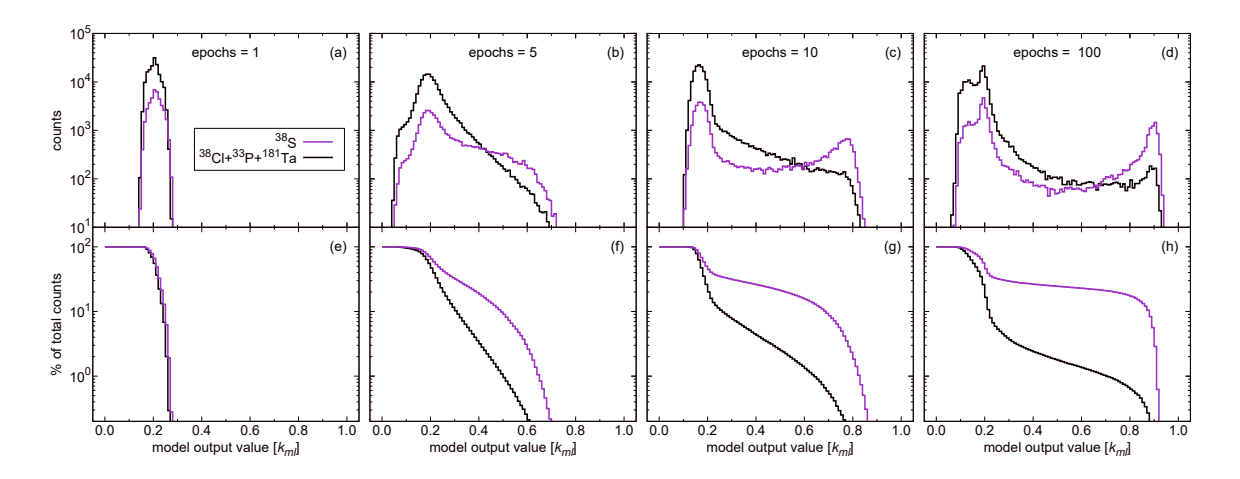


FIG. 3. (a - d) The evolution of the distribution of model output values, k_{ml} , for the training data throughout the NN model training in terms of completed epoch cycles (1, 5, 10, and 100). Purple lines correspond to the k_{ml} values of the labeled ³⁸S training data and the black lines are the corresponding values of the sum of the ³⁸Cl, ³³P, and ¹⁸¹Ta labeled training data. (e - h) The fraction of the total number of integrated counts (given in %) over the integral range starting from the k_{ml} value up through 1, i.e. $\int_{k_{ml}}^{1} dN / \int_{0}^{1} dN$, at same points during training as in (a - d).

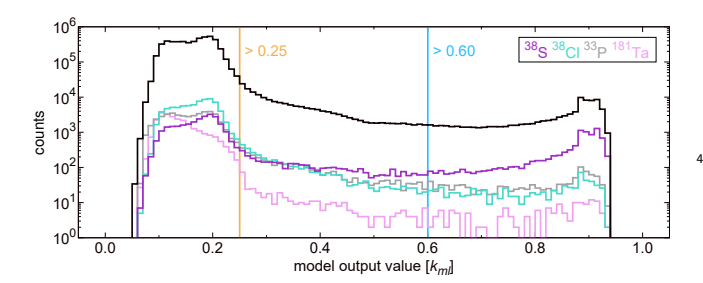


FIG. 4. The distribution of the model output values, k_{ml} , for the fully-trained NN model (epochs = 200). The black line represents the full complement of data encompassed within the manual gating regions, both labeled and un-labeled. The colored lines correspond to the final distributions of each of the separately labeled training data only (purple - 38 S, blue - 38 Cl, grey - 33 P, pink - 181 Ta). The yellow (> 0.25) and blue (> 0.60) vertical lines identify the lower-limit k_{ml} cutoff values, where the upper limit was defined = 1, that were used in the γ -ray analysis (see text for additional details).

where contaminants may have been present from 38 Cl in particular, coincidences were checked with data from the more stringent $k_{ml} > 0.60$ cut. Statistics limited the 425 observation of any higher-order γ -ray multiplicities.

The semi-alignment of magnetic sub-states provided by the near-symmetric fusion evaporation reaction was leveraged to inform on some transition multipolarities. The ratio of the γ -ray singles yields, R_{θ_2/θ_1} , was extracted from data included within the $k_{ml}>0.60$ cut. 460 Although GRETINA has essentially a continuous angular coverage, only two angular bins were used due to statistic. One was centered around $\theta_2=149^\circ$ and the other centered around $\theta_1=90^\circ$. Relative efficiency corrections 455 for each angle were determined from the γ -ray source 465

data over for the same corresponding binning regions. The uncertainty on $R_{149^{\circ}/90^{\circ}}$ was driven by statistics and the systematic uncertainties from the relative efficiency corrections. Above $E_{\gamma} > 500$ keV the systematic uncertainty due to the relative efficiency was 5%. Below $E_{\gamma} \approx 500$ keV the uncertainty was increased to $\sim 10\%$ due to a non-negligible energy dependence observed for the relative $\theta_{90^{\circ}}$ yields in the source data. Stretched-quadrupole ($\Delta J = 2, L = 2$) transitions are expected to reside above $R_{149^{\circ}/90^{\circ}} \gtrsim 1.2$, while the dipole $\Delta J \leq 1$, L = 1 counterpart transitions are more probable for $R_{149^{\circ}/90^{\circ}} \lesssim 1$ values. The known 1293-keV and 1535-keV 38 S γ -rays, both having $\Delta J = 2$, gave $R_{149^{\circ}/90^{\circ}} \gtrsim 1.2$, in agreement with expectations.

IV. EXPERIMENTAL RESULTS

A. Selection of 38 S γ -ray transitions

The γ -ray transitions attributed to ³⁸S based on the present analysis are labeled by their observed energies in the γ -ray singles spectra of Fig. 5 and they are also listed in Table II. Transitions in ³⁸S were identifiable by showing little change in their yields between the spectra with the $k_{ml} > 0.25$ cut versus the $k_{ml} > 0.60$ cut as shown in Figs. 5(a), (c), and (e). Spectra generated from the $k_{ml} > 0.60$ cut (blue) were far-removed of the contaminant lines, in particular those from ³⁸Cl, which appear prominently in the $k_{ml} > 0.25$ selection (yellow) but diminish largely for the $k_{ml} > 0.6$ selection. Note that a smooth background has been subtracted from the singles spectra in Figs. 5(a), (c), and (e). The summed recoil- γ - γ spectra ($k_{ml} > 0.6$) in the lower half of each

panel of Fig. 5, provide additional support of the associated ³⁸S transitions. The relative intensities of the ³⁸S transitions were determined from the singles spectra of the $k_{ml} > 0.60$ data. They are given in Table II, nor-470 malized to the intensity of the 1293-keV line ($\equiv 1000$). Uncertainties on the relative intensities were dominated by statistics over the systematic contributions from the peak fitting and background subtraction (< 5%) or the $_{525}$ too likely has a positive parity. energy-dependent efficiency correction (< 5%).

³⁸S level and decay scheme

475

An updated ³⁸S level and decay scheme incorporating the present data is shown in Fig. 6. Some details pertaining to the construction of specific levels or locations of transitions are given below. In general, the placement of 480 transitions into the ³⁸S decay scheme was done through the use of γ -ray and excited level energy summations, the relative γ -ray intensities (Table II), and where possible, utilizing the recoil- γ - γ coincidence data (Figs. 8). Dashed transitions or levels in Fig. 6 identify cases where 485 the coincidence data was inconclusive or where only the energy-sums were used. Newly assigned or speculative J^{π} information was extracted from the $R_{149^{\circ}/90^{\circ}}$ values (Fig. 7 and Table II), as well as transition selection rules and the propensity of the fusion evaporation reaction mechanism to populate higher-J or yrast states with increasing excitation energy.

1. The yrast even-J levels

The energies and J^{π} values for the even-J yrast levels up to $J^{\pi} = 4^{+}$ have been firmly established (0.000 MeV -0^{+} , 1.293 MeV -2^{+} , and 2.827 MeV -4^{+}). A tentative $J^{\pi} = (6_1^+)$ assignment to the 3.677-MeV level was made previously based on speculative (t,p) angular distributions [6], as well as, observation of sizeable population and a predominant decay branch to the 4_1^+ level by various in-beam reaction work [9–13]. The γ -ray coincidence data and the relative intensities extracted in the present work agree with the established 1293-, 1535-, and 850keV γ -ray cascade and arrangement [Figs. 8(a) and (b)]. $R_{149^{\circ}/90^{\circ}} \gtrsim 1.2$ values were extracted for each transition. 505 including the 850-keV γ ray, showing consistent L=2quadrupole multipolarity throughout the cascade (Fig. 7 and Table II). The assignment of the 3.677-MeV level has therefore been modified to $J = 6_1^{(+)}$, where positive parity most likely.

A coincidence relationship was observed between the 565 known yrast $J^{\pi} = 0^+ - 4^+ - 6^{(+)}$ sequence and the 2668-keV γ ray [Figs. 8(a) and (b)]. First identified in Refs. [11, 12], the 2668-keV transition has now been placed to directly feed the 3.677-MeV level from a new 515 level at 6.346 MeV. No additional transitions were observed to decay from this new level suggesting a decay branch of near $\sim 100\%$ to the $6_1^{(+)}$ level. The efficiency

corrected intensities for the 1535- and 850-keV transitions relative to the 1293-keV $[\equiv 1.00(12)]$ were 0.98(12), 0.85(11) in the 2668-keV gated γ - γ coincidence spectrum. The extracted $R_{149^{\circ}/90^{\circ}} = 1.74(19)$ value of the 2668-keV γ ray shows a clear quadrupole multipolarity. Hence, the new level at 6.346 MeV has been assigned as the yrast

Extending the even-J yrast sequence beyond J = 8with any certainty proved difficult. Exploration of the summed and individual coincidence spectra for the yrast even-J transitions revealed two possible candidate γ rays at 1617-keV and 2385-keV [Fig. 8(b)]. Any coincidence relationship between these two lines was uncertain due to the limited statistics. Coincidence with the 2668-keV transition in both cases led to their tentative placements directly feeding into the $J^{\pi} = 8^{(+)}$ 6.346-MeV level. The tentative level at 8.730 MeV has no spin-parity suggestion as the multipolarity information on the 2385-keV γ ray is inconclusive $[R_{149^{\circ}/90^{\circ}} = 1.61(73)]$ though $J \geq 8$ is most likely. The placement of the 1617-keV transition generated a level with an energy sum of <2 keV within that of the 7.963-MeV level established by the 1950-keV transition (see sub-section IV B 5 below). The 1617-keV γ -ray's $R_{149^{\circ}/90^{\circ}} < 1.0$ value favored a dipole multipolarity and the 7.963-MeV level having J = (8,9), consistent with the 1950-keV cascade.

The 2.806-MeV, 3.519-MeV, 3.615-MeV and 3.999-MeV levels

The energies of the 2.806-, 3.519-, 3.615-, and 3.99-MeV levels were previously established with J^{π} values of 2_2^+ , (1-3), $(2^+,3^+)$ and $(3^+,4^+)$, respectively (see Fig. 6.46 of Ref. [12] for example). The doublet of states around 2.8 MeV was cleared up definitively in Ref. [8] and a recent work confirmed the assignment of the 2.806-MeV level as $J^{\pi} = 2^{+}_{2}$ [20]. The 3.519-MeV level was first identified in the β -decay of ³⁸P [3] leading to a limit on J from the (2^{-}) ground state. The same level was also weakly populated in the deep-inelastic work of Refs. [11, 12]. The 3.615-MeV and 3.999-MeV levels were suggested to be part of a multiplet of levels (including the 4.437-MeV level discussed below) based on the $(\nu 0 f_{7/2} \nu 1 p_{3/2})_{J=2-5}$ configuration [10, 11].

All of the previously observed transitions from these levels have been confirmed in the present work (Fig. 5). Two new linking transitions, the 810-keV and the 788keV lines, were observed to decay from the 3.615-MeV The location of 810-keV line was established through the recoil- $\gamma - \gamma$ coincidence data with the 1513keV line. The weak 788-keV transition meets the energy requirements to link the 2.827-MeV and 3.615-MeV levels. It also showed marginal coincidence with the 384keV line and the lower-lying 1293- and 1535-keV lines. The appearance of the 1535-keV transition within the coincidence spectrum of the 384-keV line also indirectly

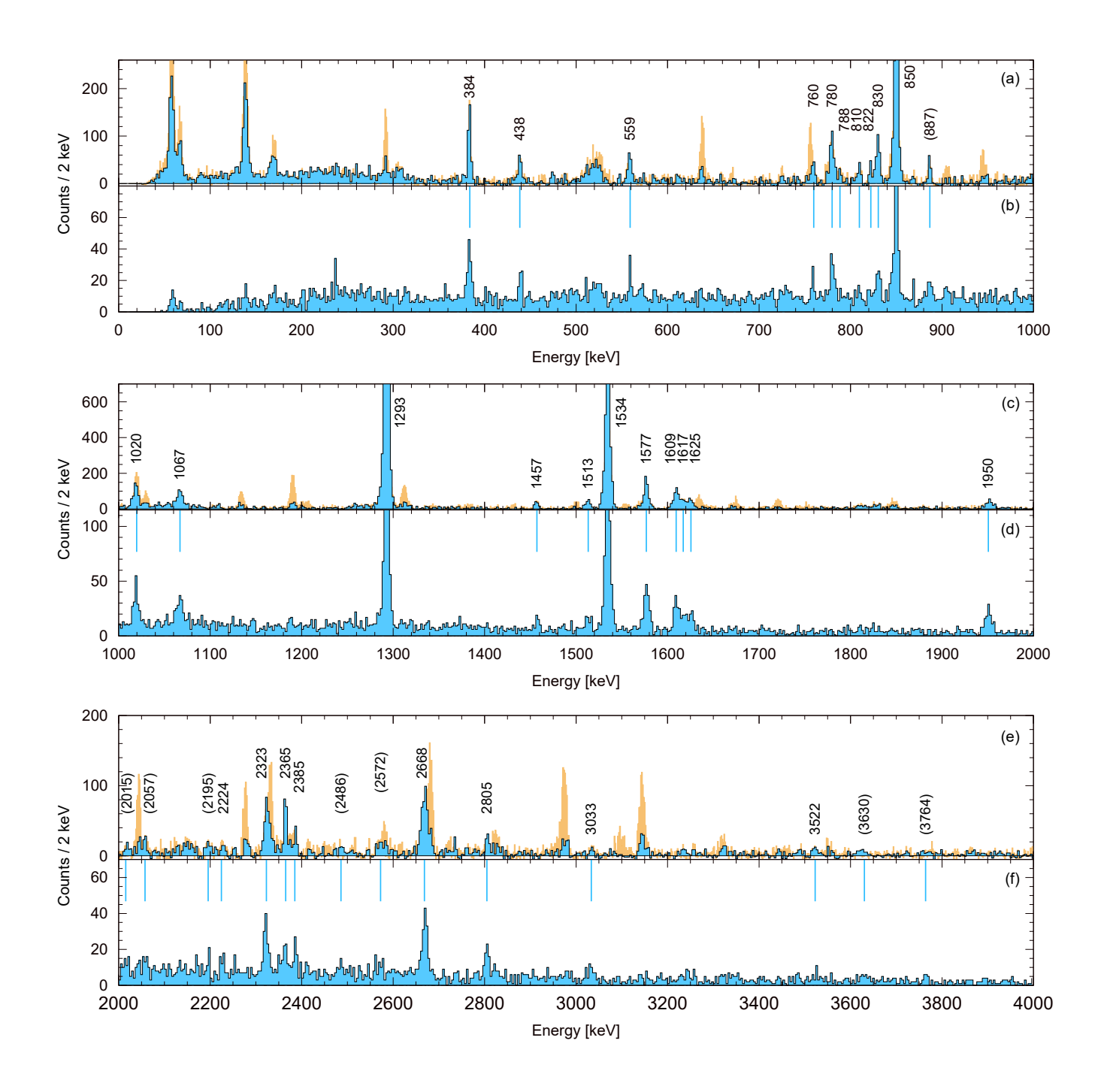


FIG. 5. (a),(c),(d) Background-subtracted γ -ray singles spectra from a model output cut of $k_{ml} > 0.6$ (blue) overlaid on a cut of $k_{ml} > 0.25$ (yellow). Transitions identified as 38 S are labeled by their energies in keV. Parenthesis indicate transitions that were unable to be placed in the level scheme (Fig. 6). (b),(d),(f) The inclusive sum of the recoil- $\gamma - \gamma$ coincidence spectra ($k_{ml} > 0.6$ cut) for all 38 S transitions identified. The blue vertical lines correspond to the labeled energies of the above histogram.

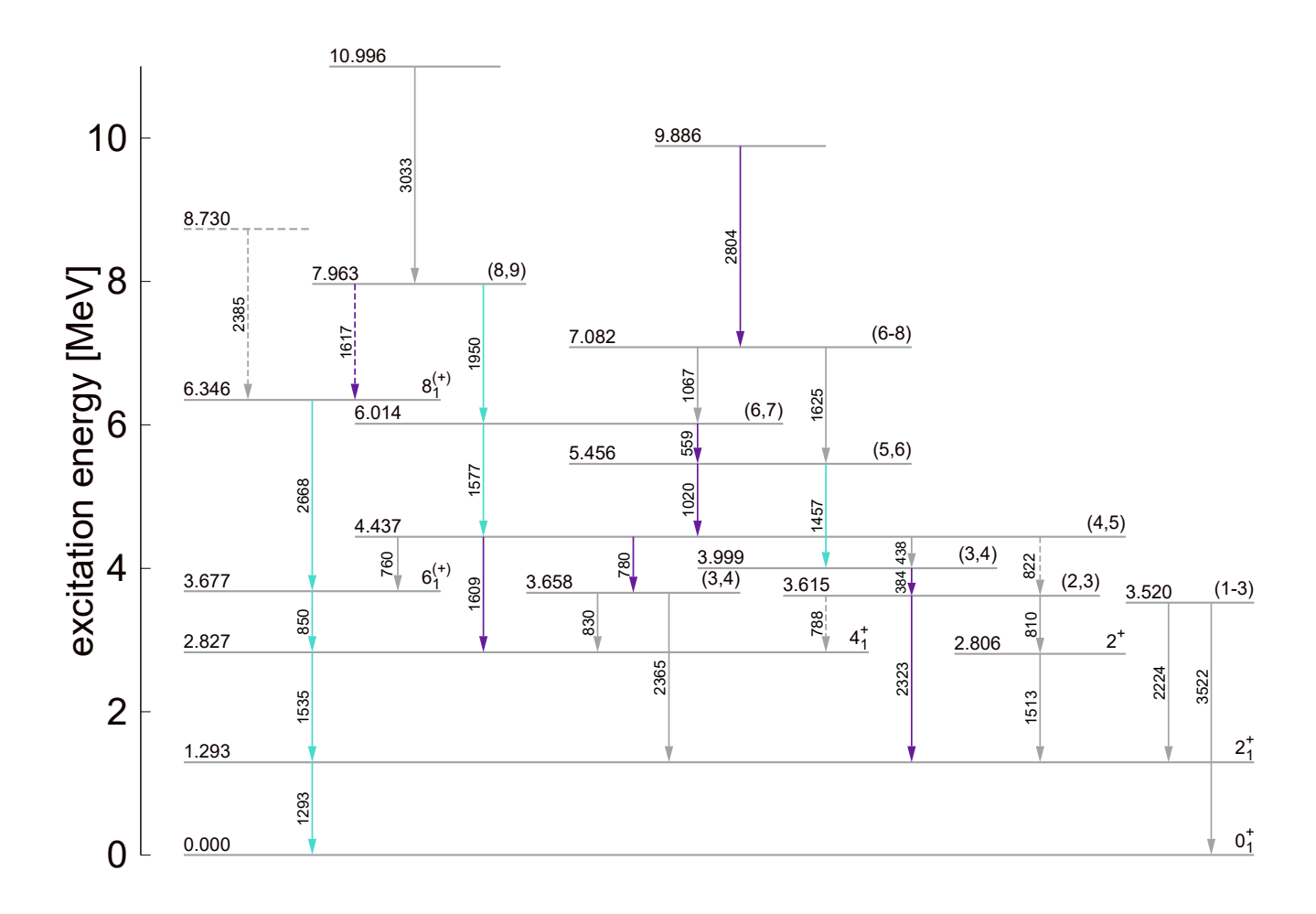


FIG. 6. The level and decay scheme of 38 S based upon the present work and other in-beam measurements. Dashed levels and transitions indicate tentative placement. Transitions in green (L=2) and purple (L=1) reflect multipolarities based on their $R_{149^{\circ}/90^{\circ}}$ values (Fig. 7 and Table II).

supported its placement.

585

No new information on the properties of the $J^{\pi}=2^{+}_{2}$ 2.806-MeV level was determined in the present work due to the limited population of this non-yrast state. The $R_{149^{\circ}/90^{\circ}}$ values for the 2323-keV and 384-keV transitions support the sequence of dipole transitions proposed in Refs. [10–12] for the 3.615-MeV and 3.999-MeV levels. There is a propensity for the higher of the two possible J-value assignments in each case due to the fusion-evaporation reaction mechanism, however, no direct empirical evidence is available to solidify this point. Therefore, the two levels remain with $J^{\pi}=(2,3)$ and (3,4).

3. The 3.657-MeV level

A new level was established at an excitation energy of 3.657-MeV and assigned with tentative spin values of

J=(3,4). Energy summations and recoil- γ - γ coincidence relations between the 830-keV, 780-keV, and 2365keV transitions with the known $4_1^+ \rightarrow 2_1^+ \rightarrow 0_1^+$ cascade were used [Fig. 8(d)]. There were no previously recorded levels having energies consistent with 3.657 MeV, although the 2365-keV was also observed in Refs. [11, 12]. The ~ 830 -keV data observed in Ref. [13] originated from the 850-keV transition but was shifted in energy due to its > 100 ps lifetime, hence, it is not the same transition as has been observed here. The tentative spin-parity range came from the limits of the 2365-keV transition to the known 2_1^+ level and the 830-keV transition to the known 600 4_1^+ level $(2 \le J \le 4)$. The $R_{149^{\circ}/90^{\circ}} = 0.81(18)$ value of the 780-keV transition favors $3 \le J \le 5$ when coupled with the possible J values of the 4.437-MeV level (see subsection IV B 4 below). The $R_{149^{\circ}/90^{\circ}} = 1.88(44)$ of the 830-keV line is not obviously consistent with either $_{605} J = (3,4) \rightarrow 4_1^+ \text{ transition.}$

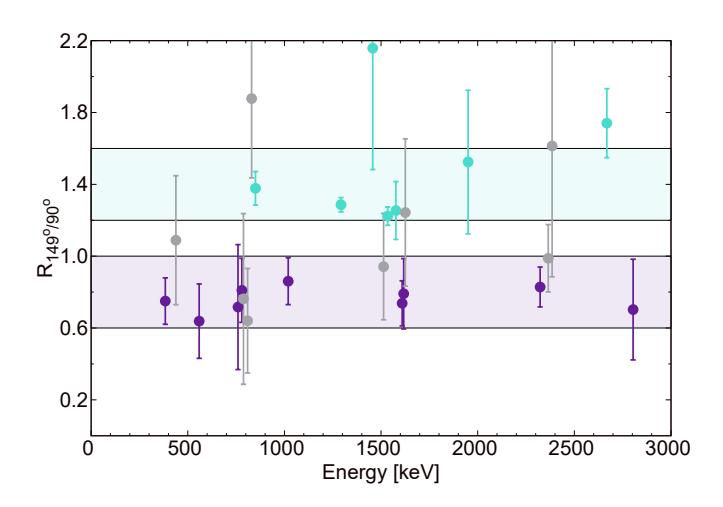
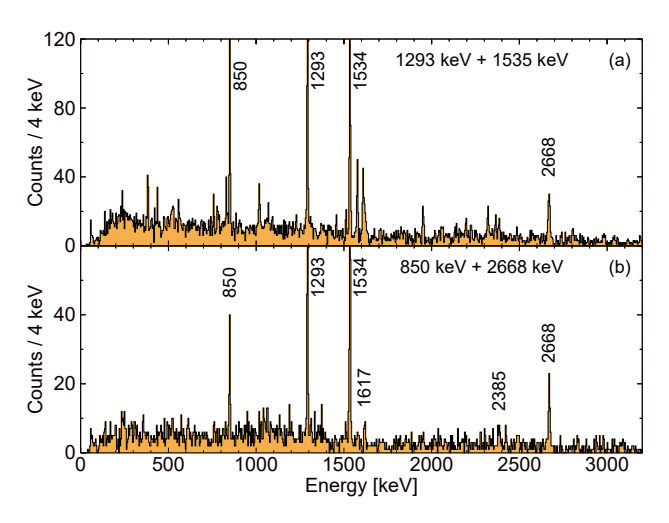


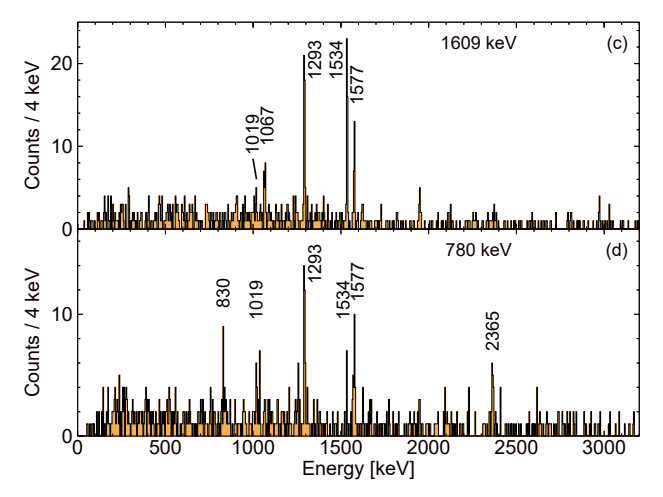
FIG. 7. The ratio of the extracted γ -ray yields centered around $\theta=149^{\circ}$ by that around $\theta=90^{\circ}$, $R_{149^{\circ}/90^{\circ}}$, for identified transitions in $^{38}{\rm S}$ as a function of their energy. The colored data points correspond to either fully-stretched quadrupole transitions residing above ≈ 1.2 (blue for multipolarity L=2) or dipole transitions residing below ≈ 1 (purple for multipolarity L=1). Grey data points were not assigned multipolarities due to large uncertainties or conflicts within the level scheme.

4. The 4.437-MeV level

A key marketplace of the $^{38}{\rm S}$ level scheme has appeared at the 4.437-MeV level. Similar levels were previously identified in the deep inelastic works of Refs. [10–12] at both 4.436-MeV and 4.437-MeV. The former was tentatively assigned $J=(4^+,5^+)$ based on theoretical arguments that the level was a member of the $(\nu 0f_{7/2}\nu 1p_{3/2})_{J=2-5}$ multiplet. The latter was only postulated based on the placement of an observed 1611-keV transition, though the two levels agreed in energy within uncertainties. A broad peak around 4.43 MeV was also observed in the heavy-ion transfer work of Ref. [5] as well as a level at 4.478(22) MeV which was given $J=(3^-,4^+)$ in the (t,p) work of Ref. [6].

The 4.437-MeV - 3.999-MeV - 3.615-MeV decay sequence suggested in Refs. [10, 11] was confirmed by the recoil- γ - γ coincidence relations between the 384-keV and 438-keV transitions. The coincidence spectra of the 780-keV and 1609-keV lines showed a number of transitions that were also found to be in coincidence with the 438-keV transition, including the 1577-keV, 1950-keV, and 1020-keV γ rays [Figs. 8(c) and (d)]. The energy summations for each possible decay path stemming from the 4.437-MeV level were in agreement to within \sim 1 keV. Therefore, within the \sim 1 keV energy uncertainty a single level at 4.437 MeV has been placed in the level scheme having four outgoing transitions (760-keV, 780-keV, 1609-keV, and 438-keV). A possible fifth transition





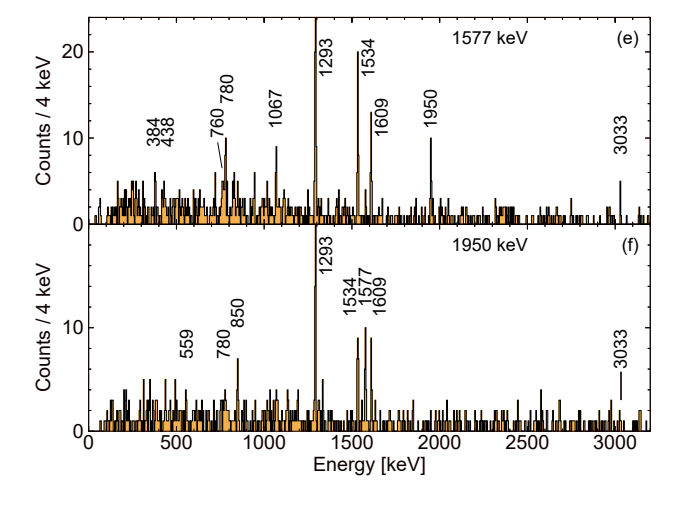


FIG. 8. Projected recoil- γ - γ coincidence spectra for $k_{ml} > 0.25$. The labels provide the γ -ray energy or energies selected for the projection. Only some of the transitions of interest have been labeled in each spectra. No background subtractions have been applied.

through the 822-keV γ -ray was also included based on 635 energy arguments alone. The 1577-keV and 1020-keV gated recoil- γ - γ coincidence projections, both of which were found to feed the 4.437-MeV level directly, showed coincidences with the 760-keV, 780-keV, 1609-keV and 438-keV γ rays. Unfortunately, a check for consistency between relative yields for the exiting transitions was 695 not possible due to the low statistics and background counts in the γ -ray coincidence data. The 1950-keV and 1625-keV lines, and to a lesser extent the 559-keV line, each had a coincidence spectrum which supported a sin-645 gle level at 4.437-MeV [Figs. 8(e) and (f)].

The placement of only a single level at 4.437-MeV is in contrast to the proposed levels in Table 6.15 of Ref. [12] but supported by the coincidence data and within the uncertainties of that work. The relative intensities between the 438-keV and 1609-keV lines are consistent between the two works. The 4.437-MeV level has been given a tentative range of J = (4,5) with the J = (5) assignment slightly favored due to the reaction mechanism and multipolarity information. From the linking transitions between the 4.437-MeV level to levels with known J^{π} , 710 spins of J = (4-6) were possible. The 760-keV transition placement was critical as it set the lower limit. The 1609-keV $R_{149^{\circ}/90^{\circ}} = 0.74(13)$ ratio favors a dipole multipolarity and therefore, J < 6. The 760-keV transition 660 has a suggestive $R_{149^{\circ}/90^{\circ}} = 0.72(35)$ ratio of a dipole 715 of the 1020-keV transition $(R_{149^{\circ}/90^{\circ}} = 0.86(11))$ transition and is consistent with values of $(5) \rightarrow 6^{(+)}$ for the 4.437-MeV and 3.677-MeV levels. The observed dipole multipolarity of the 780-keV transition was also consistent with either spin do to the uncertain final state spin of the 3.657-MeV level, J = (3,4). The 438-keV and 822-keV multipolarities were inconclusive. It is unclear whether the 4.437-MeV level is the same as that observed in the (t,p) work of Ref. [6]. If it is, then a $J=(4), \pi=+$ assignment could be made as the (t,p)₆₇₀ proton angular distributions rule out L=5 and the 760keV transition rules out a $J^{\pi} = 3^{-}$ assignment.

The 5.456-MeV, 6.014-MeV, 7.081-MeV, and 7.963-MeV levels

Levels with energies of 5.456 MeV, 6.014 MeV, 7.081 675 MeV, and 7.963 MeV were identified in the present data. Only the 6.014-MeV level had parallels with some previous work which found levels at 6.020(30), 6.000(30), and 6.006 MeV [3, 5, 6]. It is likely that a common level having $J=(3^-)$ was observed in both the (t,p) and β decay works at 6.006 MeV. However, this does not ap- 735 have been placed into the ³⁸S level scheme based on the pear to be the same level observed in the present work due to disagreements in possible J values. The strongest of the transitions comprising these new levels, the 1577keV γ ray, was first observed in the deep inelastic work of 685 Ref. [11] but here placed higher in the level scheme than 740 postulated in their Table 6.15.

The combination of recoil- γ - γ coincidence data with the 3.999-MeV and 4.437-MeV levels, as well as energy

summations, led to the placement of the eight transi-690 tions (one as tentative) to or from these new levels. A lack of presence of the 438-keV γ ray in the 1457-keV gated γ -ray spectrum and the relation between the 4.437-MeV level and the 1020-keV transition, established the 5.456-MeV level. The appearance of the 1625-keV transition in both the 1457-keV and 1020-keV gated spectra, and vice-versa, determined its location directly feeding the 5.456-MeV level. The 1950-keV to 1577-keV sequence was established through commensurate coincidences with one another as well as their observed intensities from the 1609-keV gated coincidence spectrum [Fig. 8(c)]. The relatively weak 559-keV transition linking the 6.014-MeV and 5.456-MeV levels was placed primarily based on its energy agreement, though it did also show tentative evidence for a coincidence relation with the 1950-keV [Fig. 8(f)] and 1020-keV transitions. Finally, the 1067-keV γ -ray was observed to be at least a doublet. One 1067-keV transition was in coincidence with the 1577-keV transition and its energy was consistent with the difference between the 7.082-MeV to 6.014-MeV levels. However, the placement of any further 1067keV γ -rays was not able to be reconciled in the present work.

The 5.456-MeV level has been tentatively assigned (5,6) based on the extracted dipole nature and the quadrupole nature of the 1457-keV transition $(R_{149^{\circ}/90^{\circ}} = 2.16(67))$ which feed the J = (4,5) 4.437-MeV and J = (3,4) 3.999-MeV levels, respectively. The extracted multipolarities of the 1577-keV (quadrupole) $_{720}$ and 559-keV (dipole) transitions similarly limit the Jrange of the 6.014-MeV level to J = (6,7). The 1950keV transitions $R_{149^{\circ}/90^{\circ}} = 1.52(40)$ ratio is consistent with a quadruple transition building upon the 6.014-MeV level giving J = (8,9) for the 7.963-MeV level. As noted above in sub-section IV B 1, the suggested J values for the 7.963-MeV level are consistent with the multipolarity of the tentatively placed 1617-keV transition which feeds into the $J=8_1^{(+)}$ 6.346-MeV level. Finally, only a limit of J = 5 - 8 could be surmised for the 7.081-MeV level due to the doublet nature of the 1067-keV transition and the non-distinct $R_{149^{\circ}/90^{\circ}}$ value of the 1625-keV transition.

Levels residing above 9.5 MeV in excitation energy

Two additional levels at 9.885 MeV and 10.996 MeV observed 2804-keV and 3033-keV γ rays, respectively. Due to the weak nature of these higher lying states, their placement was most apparent in the γ -ray coincidence data provided by the $k_{ml} > 0.6$ recoil selection, though the 3033-keV line is visible in Fig. 8(e). The 2804-keV transition was within a few keV of the known 2.806-MeV 2_2^+ level. However, it showed clear coincidences with the 1293-keV and 1535-keV transitions amongst others, lead-

ing to its placing higher in the level scheme. Furthermore, no evidence for a \sim 2806-keV transition appeared in the 810-keV gated coincidence data which clearly showed the 1513-keV line. The 2804-keV line did appear in the summed γ -ray spectrum consisting of the combined 559-1020-, 1067-, and 1625-keV gated transitions and the 750 2804-keV coincidence gated spectrum reciprocated the stronger three of these transitions as well. The 2804-keV line also showed a preference for a dipole multipolarity. however, no J information could be concluded for the 805 9.885-MeV level as only range of spins was placed on the 755 7.081-MeV level.

It is unlikely that the presently observed 3033-keV transition is the same as the 3010-keV line observed in the deep inelastic work [11, 12] due to the energy differences. A clear coincidence was observed between the 3033-keV line and the 1293-keV transition which eliminated the possibility for direct ground-state feeding. The summed γ -ray coincidence spectrum comprised of both 1577-keV and 1950-keV gates demonstrated a clear coincidence with the 3033-keV line. A limit of J > 8 could 765 be made for the 10.996-MeV level based on the reaction mechanism and the tentative assignment of the 7.963-MeV level.

7. Unplaced γ -ray transitions

820

There were a sub-set of γ -ray transitions which were 770 identified as belonging to the ³⁸S decay scheme but were unable to be placed. They have been labeled with parenthesis around their energies in Table II. Of these, it is probable that the 2057-keV, 2195-keV, 2485-keV, and 2572-keV, correspond to transitions which have been previously listed in the deep inelastic work of Ref. [11, 12]. It may be speculated that the 2057-keV transition feeds the 1.293-MeV level and that the 2195-keV level feeds the $J = 4^{+}$ 2.827-MeV state, corresponding to the 3.375(17)-MeV and 5.064(27)-MeV levels observed in Ref. [6]. However, no coincidence data was available to weigh in on these hypotheses.

\mathbf{V} . **CALCULATIONS & DISCUSSION**

The low-lying positive-parity structure of ³⁸S has been well described by the coupling of a pair protons occupying the $1s_{1/2}$ and $0d_{3/2}$ orbitals (outside of a filled $0d_{5/2}$ orbital) and a pair of neutrons occupying primarily the $0f_{7/2}$ and $1p_{3/2}$ orbitals. Within this space, the combination of $\pi(1s_{1/2}0d_{3/2})_{J=1,2}$, $\pi(1s_{1/2})_{J=0}^2$ or $\pi(0d_{3/2})_{J=0,2}^2$ configurations with neutron 790 $\nu(0f_{7/2}1p_{3/2})_{J=2-5},\ \nu(0f_{7/2})_{J=0,2,4,6}^2,\ {
m or}\ \nu(1p_{3/2})_{J=0,2}^2$ 845 configurations provide J values ranging from 0^+-8^+ . Excited levels reaching $J^{\pi} > 8^{+}$ are most readily accessible from either the promotion of a $0d_{5/2}$ proton into the $1s_{1/2}0d_{3/2}$ orbitals within the 1s0d shell or from the pro-

shell, 2p-2h excitations. Though contained with the valence space of previous calculations, i.e. the SDPF-MU and the sdpf-u interactions, there were no published predictions of the locations of $J^{\pi} > 6^{+}$ levels based on $\pi(0d_{5/2})^{-1}$ configurations. Similarly, high-J states based on 2p-2h configurations were also unavailable. However, lower-J values pf 2p-2h character have been predicted to appear at around 3–4 MeV in excitation energy [6, 7]. Experimentally, there are a few possible candidates for such 2p-2h states, for instance levels with natural parity that were weakly populated in the past (t, p) work, but there are no concrete correspondences.

The lowest-lying negative parity states are expected to also have single-particle configurations built upon on odd numbers of particle hole excitations from the 1s0dshells into the 0f1p shells (1p-1h). Experimentally, a number of candidates exists for $\pi = -$ levels based on the β -decay work and the (t,p) measurement data. The lowest of these is around ~ 3.5 MeV which is below the 815 $\nu(0d_{3/2}^{4-n}0f_{7/2}^{n+2})^6$, n= odd model-space constrained shellmodel calculations presented in Ref. [7] and well below the weak-coupling prediction considering ³⁵S⊗⁴³Ca [6] $(\sim 4.5-5 \text{ MeV}).$

Shell-model calculations based on the FSU interaction

To further interpret the level and decay scheme of 38 S, shell-model calculations where completed using an empirically-adjusted effective interaction, the so-called FSU [28] interaction. This interaction was developed to prosper in the vicinity of ³⁸S having a valance space for particles within both the 1s0d and 0f1p shells. The FSU interaction was constructed with an emphasis on describing intruder states consisting of particle-hole (np - nh)excitations originating from within the 1s0d shell and then being promoted into the adjacent 0p or 0f1p subshells [28]. The FSU interaction has been successful in describing, amongst other things, levels based on the $\pi 1s0d$ - and $\nu 0f1p$ -shell configurations [40–42], and in particular both the normal and intruder levels in ³⁸Cl and ^{38,39}Ar [38, 43].

Positive parity 0p-0h states in ³⁸S were calculated using the FSU interaction and requiring 8 valance protons to be confined within the 1s0d shell and the 2 valence neutrons to be confined within the full 0f1p shell. The interaction was also used to provide predictions of negative parity (1p-1h) states and additional positive parity (2p-2h) states by allowing fixed-numbers of excitations (protons or neutrons) from within the 1s0d orbitals across the N=20 shell gap and into the 0f1p orbitals. No mixing was allowed between the positive parity 0p - 0hand 2p-2h states. A sub-set of the calculated levels are presented in Fig. 9 including the two lowest-energy 0p - 0h states through $J^{\pi} = 10^{+}$. The lowest energy $\pi = -$ level for each spin up to J = 10 is given for the ₇₉₅ motion of pairs of 1s0d particles into the upper 0f1p ₈₅₀ 1p-1h calculations and similarly for even- J^+ states re-

TABLE II. Identified γ -ray transitions in 38 S based on the present work. The γ -ray energies, E_{γ} , have uncertainties of \sim 0.5-1 keV. The relative intensities have been normalized to the 1293-keV transitions (\equiv 1000). The ratio of the angular yields, $R_{149^{\circ}/90^{\circ}}$, and the relative intensities, I_{γ} , were extracted from data based on the $k_{ml} > 0.60$ cut and include statistical and systematic uncertainties.

$E_i [MeV]$	J_i^π	$E_{\gamma} [keV]$	I_{γ}	$E_f [MeV]$	J_f^π	$R_{149^{\circ}/90^{\circ}}$
0.000	$0_1^+ \ 2_1^+ \ 2_2^+ \ 4_1^+$	_	_	_	-	_
1.293	2_{1}^{+}	1292.7	$\equiv 1000$	0.000	0_{1}^{+}	1.29(5)
2.806	2_{2}^{+}	1513.1	38(6)	1.293	2_{1}^{+}	0.94(30)
2.827	4_{1}^{+}	1534.5	598(35)	1.293	2_{1}^{+}	1.22(5)
3.520	(1-3)	2224.4	19(5)	1.293	2_{1}^{+}	_
		3522.3	24(6)	0.000	0_1^{+}	_
3.615	(2,3)	788.3^{a}	11(3)	2.827	4_{1}^{+}	0.76(48)
		809.6	14(3)	2.806	2_{2}^{+}	0.64(29)
		2322.8	140(12)	1.293	$2_{1}^{\tilde{+}}$	0.83(11)
3.657	(3,4)	830.2	37(4)	2.827	4_{1}^{+}	1.88(44)
		2364.8	89(9)	1.293	2_{1}^{+}	0.99(19)
3.677	$6_1^{(+)}$	850.1	201(12)	2.827	$0_1^+ \ 2_1^+ \ 2_1^+ \ 2_1^+ \ 2_1^+ \ 0_1^+ \ 4_1^+ \ 2_1^+ \ 4_1^+ \ 2_1^+ \ 4_1^+ \ 4_1^+$	1.38(9)
3.999	(3,4)	383.6	39(5)	3.615	(2,3)	0.75(13)
4.437	(4,5)	438.3	18(3)	3.999	(3,4)	1.10(36)
	(/ /	759.7	16(2)	3.677	$6_1^{(+)}$	0.72(35)
		779.8	40(4)	3.657	(3,4)	0.81(18)
		822.0^{a}	15(4)	3.615	(2,3)	_
		1609.3	86(7)	2.827	4_1^+	0.74(13)
5.456	(5,6)	1019.6	81(9)	4.437	(4,5)	0.86(11)
	(/ /	1457.0	28(6)	3.999	(3,4)	2.16(67)
6.014	(6,7)	558.9	18(4)	5.456	(5,6)	0.64(21)
		1576.7	112(6)	4.437	(4,5)	1.25(16)
6.346	$8_1^{(+)}$	2668.2	194(25)	3.677	$6_1^{(+)}$	1.74(19)
7.081	(6-8)	$1066.9^{\rm b}$	69(6)	6.014	(6,7)	_
	()	1625.4	45(5)	5.456	(5,6)	1.24(41)
7.963	(8,9)	$1617.3^{\rm a}$	40(5)	6.346	$(5,6)$ $8_1^{(+)}$	0.79(20)
1.000	(0,0)	1950.3	48(6)	6.014	(6,7)	1.52(40)
8.730°	_	$2384.7^{\rm a}$	43(7)	6.346	8 ₁ ⁽⁺⁾	1.61(73)
9.885	_	2804.0	40(8)	7.081	(6-8)	0.70(28)
10.996	_	3032.6	17(7)	7.963	(8,9)	-
_	_	(887)	21(5)	-	(0,0)	_
_	_	(2015)	17(5)	_	_	_
_	_	(2057)	34(6)	_	=	_
_	_	(2195)	26(6)	=	_	_
_	_	(2486)	25(6)	_	_	_
_	_	(2572)	34(10)	_	_	_
-	_	(3630)	14(5)	-	-	_
_	_	(3764)	13(4)	_	_	_

^a Tentatively placed transition.

sulting from the 2p-2h calculations.

The present calculations carried out with the FSU interaction gave similar low-lying level energies and orderings as the previous calculations presented in Refs. [6, 7, 13, 17, 20]. The yrast $J^{\pi}=8^+$ level is calculated to have an energy of 6.32 MeV followed by the lowest-lying 0p-0h 10^+ level at around 11 MeV. Positive parity 2p-2h excitations appear at ~ 3 MeV in excitation energy in Fig. 9. However, the 2p-2h even-J states do not begin to compete in energy with the 0p-0h levels so as to become yrast states up to at least $J^{\pi}=10^+$.

The FSU interaction also predicts the first 1p-1h states $(J^{\pi}=3^{-}-5^{-})$ in the 4.2-4.9 MeV energy regime, consistent with previous model predictions. The negative parity 1p-1h states are predicted to achieve the lowest-energy spin values around J=9 or 10, near 8.5 MeV in excitation energy, ~ 1 MeV below the predicted 0p-0h and the 2p-2h 10^{+} levels.

^b Identified as a doublet.

^c Level placement is tentative.

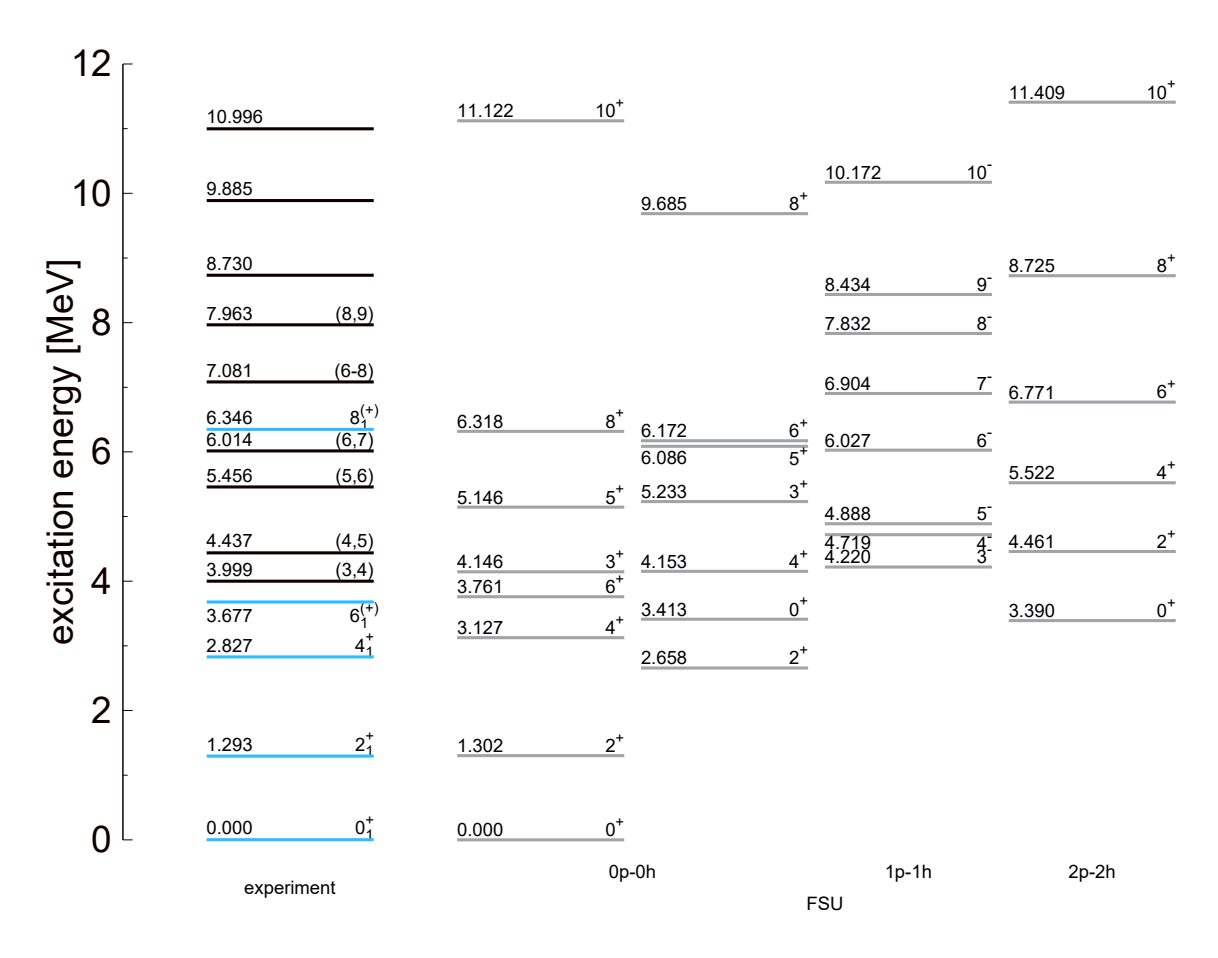


FIG. 9. A sub-set of the experimental excited-state levels in 38 S are presented along with J^{π} assignments where available. Calculated levels based on the FSU [28] interaction in which the protons were confined to the 1s0d shell and neutrons to the 1p0f shell are labeled as 0p-0h. Those that allowed for one or two particle-hole excitations across the N=20 shell gap, from within the 1s0d shell to the 0f1p shell, are labelled by 1p-1h or 2p-2h, respectively. Only a sub-set of the calculated levels are also shown (see text for additional details).

B. The even-J yrast states

In addition to the excitation energies plotted in Fig. 9, 890 the energies and calculated occupancies for the even- J^+ yrast levels up to $J^{\pi} = 10^{+} (0p - 0h)$ are also shown in Fig. 10. The calculations well reproduce the excitation energies for the $J^{\pi} = 2^+, 4^+, 6^+$ and 8^+ levels, 875 assuming positive parity for the latter two experimentally. The states with $J \leq 6^+$ show mixed but near constant proton $1s_{1/2}0d_{3/2}$ occupancies while the neutron configurations evolve with increasing J from mixed $0f_{7/2}1p_{3/2}$ occupancy to a pure $(0f_{7/2})^2$ configuration. $_{880}$ There is a sizeable amount (~ 0.5 nucleons) of $1p_{3/2}$ predicted in the 0_1^+ and 2_1^+ states. This occupancy similar to the SDPF-MU predictions shown in Fig. 20 of Ref. [13]. As discussed in Refs. [17, 18] the presence of the $\nu 1p_{3/2}$ occupancy is required in order to generate the appropriate amount of coherent proton contributions, through increased $\pi 1s_{1/2}0d_{3/2}$ occupancy, to correctly reproduce 905

the near zero $2_1^+ \to 0_1^+$ g-factor. As noted in the introduction (Sec. I), the $\nu 1p_{3/2}$ occupancy deviates from the simple $(1f_{7/2})_{J=0,2,4,6}^2$ seniority $\nu=2$ picture for the low-lying even-J multiplet for these two levels. However, the seniority scheme appears to be mostly restored at higher J according to the FSU interaction (Fig. 10). In order to generate spins of $J^{\pi}=6^+-10^+$ within the 0p-0h space, a pure $\nu 0f_{7/2}^2$ neutron configuration develops out of the demand for increased angular momentum. Specifically, inclusion of any $1p_{3/2}$ neutrons is limited to $J_{max}=5\hbar$ from the configuration $(0f_{7/2}1p_{3/2})_{J=2-5}$.

In accordance with Fig. 10 the predominant factor determining the relative energy spacing between the 6^+ – 8^+ – 10^+ levels is the arrangement of the proton occupancies. Starting with $(0f_{7/2})_{J=6}^2$ from the neutrons, there is a migration in the proton occupancy from the $1s_{1/2}$ into the $0d_{3/2}$, gaining $2\hbar$ in angular momentum, which extends $J^{\pi}=6^+$ up to 8^+ . The experimental spacing between the $J^{\pi}=6^+-8^+$ levels, $\Delta E_x=2.67$ MeV, is well

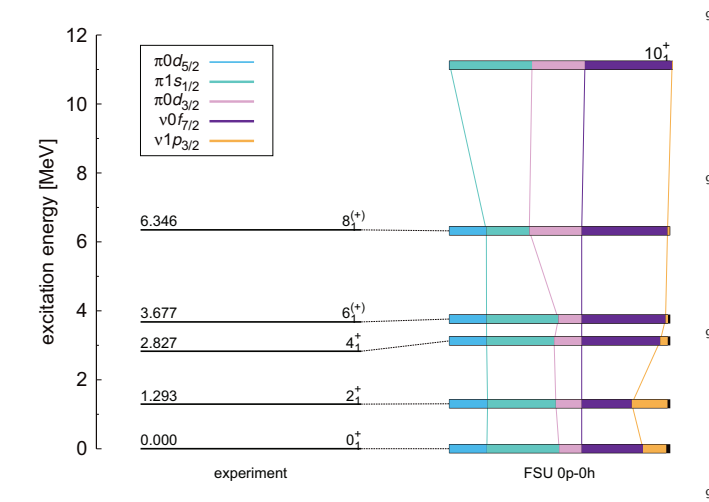


FIG. 10. The excitation energies and calculated occupancies of the even- J^+ yrast states in ³⁸S through $J_{max} = 10^+$. The relative occupancies for the orbitals of interested are labelled by color and connected by lines starting at $J = 6^+$ to highlight their evolution. The $\pi 0d_{5/2}$ occupancy is only for the '6-th' proton, i.e. an occupancy of one represents a filled $\pi 0d_{5/2}$ orbital while zero represents an occupancy of 5.

reproduced by the FSU interaction, $\Delta E_x = 2.56$ MeV. 960 It can be concluded, unsurprisingly, that the FSU interaction has a solid grasp on the description of the proton $1s_{1/2} - 0d_{3/2}$ single-particle energies and associated 910 matrix elements. One method to construct a $J^{\pi} = 10^{+}$ level is through the excitation of a proton from within the $\pi 0d_{5/2}$ orbital into the $\pi 1s_{1/2}$ orbital where the $(0d_{5/2})^{-1}$ proton hole provides the additional angular momentum. 965 The FSU interaction predicts this configuration to be vrast at 11.122 MeV. A second option for generating $J^{\pi} > 8^{+}$ levels is through 2p - 2h configurations. The addition of two neutrons into the $0f_{7/2}$ and $1p_{3/2}$ orbitals increases the neutron J_{max} contribution to $J_{max} > 6$ via ₉₂₀ The lowest-lying 2p-2h 10⁺ state predicted by the FSU interaction is only $\sim 300 \text{ keV}$ above its corresponding 0p - 0h level, hence, it is likely there is large mixing taking place between these two configurations. Unfortunately, no solid candidate was empirically determined for 975 925 the yrast 10⁺ level, though the state at 10.996 MeV is in the approximate energy range of the two predicted levels.

The neutron 0f1p shell states

The coupling of a single neutron in each of the $0f_{7/2}$ and $1p_{3/2}$ orbitals results in a multiplet of possible states 930 ranging from $J=2^+-5^+$. While the lower spins of this multiplet are susceptible to mixing, a clear correspondence to these configurations was found with the FSU interaction calculations for the 5_1^+ and 4_2^+ levels at 5.146 MeV and 4.153 MeV, respectively. The calculated 985 event recoil selection. In addition, a number of other new

935 proton occupancies are similar between the two levels $(1s_{1/2}^{\sim 1.5} \text{ and } 0d_{3/2}^{\sim 0.5})$, and the ground state for that matter. The neutron occupancies, $0f_{7/2}^{\sim 1.2}$ and $1p_{3/2}^{\sim 0.7}$, are also similar and are roughly the expected one-to-one ratio. There is a predicted 3_1^+ level by the FSU interaction at 4.146 MeV that is a possible member of the multiplet, though it is impacted by mixing resulting in variations in the proton occupancy and an increase of 0.2 in the $0f_{7/2}$

Assuming that the 5_1^+ level has a reasonably pure $_{945}$ $0f_{7/2}^11p_{3/2}^1$ neutron configuration and the 6_1^+ level has a nearly pure $(\nu 0 f_{7/2})^2$ configuration, the relative energy spacing between these levels is dependent upon the description of the 0f-1p two-body matrix elements and their single-particle energies. The calculated energy difference between the 5_1^+ and 6_1^+ states is $\Delta E_x \approx 1.4$ MeV. There are series of experimental levels at 3.615 MeV, 3.999 MeV, and 4.437 MeV, that have been eluded to as belonging to this $(0f_{7/2}1p_{3/2})_{J=2-5}$ multiplet [10-12]. Including these levels as the $J^{\pi} = 2 - 4^{+}$ members, and the newly established level at 5.456 MeV as a possible 5⁺ candidate, there is a consistent (though not unique) picture between theory and experiment. This scenario gives $\Delta E_x \approx 1.8 \text{ MeV}$ for the energy difference between the experimental 5_1^+ and 6_1^+ levels, which suggests some discrepancy with the calculations ($\approx 400 \text{ keV}$). However, there are a number of other similarly plausible corresponding assignments for the observed 5.456 MeV level with the calculations, including the calculated 5_2^+ , 5_1^- , 6_2^+ , and 6_1^- levels.

Other possible correspondences between the observed and calculated levels

The measured state at 4.437 MeV has additional counterparts in the calculations beyond the suggested $J^{\pi} = 4^{+}$ assignment and its membership in the the $(0f_{7/2})_{J_{max}=8}^4$ and $(0f_{7/2}1p_{3/2})_{J_{max}=9}^4$ configurations. $_{970}$ $(0f_{7/2}^11p_{3/2}^1)_{J=2-5}$ multiplet discussed above. In particular, the relatively large amount of fractional incoming and outgoing yield through the level may suggest it is a low-lying intruder state. The calculated $J^{\pi} = 4^{-}$ and 5^{-} states are nearby at $\sim 4.7 - 4.9$ MeV. Based on energy arguments alone, the subsequent 6.014-MeV and 7.963-MeV levels, each connected via quadrupole transitions (Fig. 7 and Table II) agree best with the $J^{\pi} = 6^{-}$ and 8^{-} levels at 6.027 and 7.832 MeV. Though a lowering of the calculated $\pi = -$ states on the order of $\sim 300\text{-}400 \text{ keV}$, would also create a viable scenario for the $5^- - 7^- - 9^$ sequence.

VI. SUMMARY & CONCLUSIONS

The even-J yrast levels in $^{38}\mathrm{S}$ were extended up to $J^{\pi} = 8^{(+)}$ based on in-beam γ -ray data and event-by-

excited levels, decay sequences, and possible spin-parities were deduced. Excited levels were populated in a fusion evaporation reaction, the in-beam γ -rays were detected by the Gretina array, and the recoil selection was carried out by the FMA and relied upon the incorporation of machine-learning based analysis techniques. Shell-model calculations based on the FSU interaction [28] well re- 1000 produced the yrast sequence and provided a number of possible scenarios for other corresponding states. In particular, the calculations gave a proper description of the measured energy spacing between the 6_1^+ – 8_1^+ levels and is directly related to the migration of proton occupancy 1005 from the $\pi 1s_{1/2}$ orbital into the $\pi 0d_{3/2}$ orbital.

VII. ACKNOWLEDGMENTS

This material is based upon work supported by the U.S. Department of Energy, Office of Science, Office of Nuclear Physics, under Contracts No. DE-AC02-06CH11357 (Argonne), DE-FG02-94ER40848 (UML), XXX, and XXX. This research used resources of ANL's ATLAS facility, which is a DOE Office of Science User Facility.

- [1] D. R. Nethaway and A. A. Caretto, New isotope, sulfur-38, Phys. Rev. 109, 504 (1958).
- (2022), evaluated Nuclear Structure Data File (ENSDF) Retrieval, Web site: www.nndc.bnl.gov/ensdf.

1055

1010

1020

1025

1035

- [3] J. P. Dufour, R. Del Moral, A. Fleury, F. Hubert, D. Jean, M. S. Pravikoff, H. Delagrange, H. Geissel, and K. H. Schmidt, Beta decay of17c, 19n, 22o, 24f, 26ne, 32al, 34al, 35-36si, 36-37-38p, 40s,Z. Phys. A **324**, 487 (1986).
- [4] L. Fifield, M. Hotchkis, P. Drumm, T. Ophel, G. Putt, and D. Weisser, The mass and low-lying levels of 40cl. Nucl. Phys. A **417**, 534 (1984).
- W. A. Mayer, W. Henning, R. Holzwarth, H. J. Körner, G. Korschinek, G. Rosner, and H. J. Scheerer, Mass ex- 1065 cess and excited states of neutron-rich silicon, phosphorus and sulphur isotopes, Z. Phys. A 319, 287 (1984).
- [6] N. J. Davis, J. A. Kuehner, A. A. Pilt, A. J. Trudel, M. C. Vetterli, C. Bamber, E. K. Warburton, J. W. Olness, and S. Raman, States of ³⁸S from the ³⁶S(t,p)³⁸s reaction, ¹⁰⁷⁰ Phys. Rev. C **32**, 713 (1985).
- [7] J. W. Olness, E. K. Warburton, J. A. Becker, D. J. Decman, E. A. Henry, L. G. Mann, and L. Ussery, $^{36}\mathrm{S}(t,p\gamma)^{38}\mathrm{s}$ reaction, Phys. Rev. C 34, 2049 (1986).
- [8] E. K. Warburton, D. E. Alburger, and G. Wang, Confir- 1075 [16] mation of the 2805-kev level of ³⁸S, Phys. Rev. C **36**, 429 (1987).
 - B. Fornal, R. H. Mayer, I. G. Bearden, P. Benet, R. Broda, P. J. Daly, Z. W. Grabowski, I. Ahmad, M. P. Carpenter, P. B. Fernandez, R. V. F. Janssens, 1080 T. L. Khoo, T. Lauritsen, E. F. Moore, and M. Drigert, Gamma ray studies of neutron-rich sdf shell nuclei produced in heavy ion collisions, Phys. Rev. C 49, 2413
- 1040 [10] J. Ollier, The yrast spectroscopy of neutron-rich nuclei 1085 produced in deep-inelastic processes, Ph.D. thesis, University of Paisley (2004).
- [11] Z. M. Wang, R. Chapman, X. Liang, F. Haas, M. Bouhelal, F. Azaiez, B. R. Behera, M. Burns, E. Caurier, L. Corradi, D. Curien, A. N. Deacon, 1090 [18] A. D. Davies, A. E. Stuchbery, P. F. Mantica, P. M. 1045 Z. Dombrádi, E. Farnea, E. Fioretto, A. Gadea, A. Hodsdon, F. Ibrahim, A. Jungclaus, K. Keyes, V. Kumar, A. Latina, N. Mărginean, G. Montagnoli, D. R. Napoli, F. Nowacki, J. Ollier, D. O'Donnell, A. Papenberg, G. Pollarolo, M.-D. Salsac, F. Scarlassara, J. F. Smith, 1095 1050 K. M. Spohr, M. Stanoiu, A. M. Stefanini, S. Szilner,

- M. Trotta, and D. Verney, Intruder negative-parity states of neutron-rich 33 Si, Phys. Rev. C 81, 064301 (2010).
- [12] Z. Wang, γ -ray spectroscopy of neutron-rich silicon and sulphur nuclei using grazing reactions, Ph.D. thesis, University of West Scotland (2010).
- [13] E. Lunderberg, A. Gade, V. Bader, T. Baugher, D. Bazin, J. S. Berryman, B. A. Brown, D. J. Hartley, F. Recchia, S. R. Stroberg, D. Weisshaar, and K. Wimmer, In-beam γ -ray spectroscopy of ^{38°42}S, Phys. Rev. C **94**, 064327 (2016).
- [14] H. Scheit, T. Glasmacher, B. A. Brown, J. A. Brown, P. D. Cottle, P. G. Hansen, R. Harkewicz, M. Hellström, R. W. Ibbotson, J. K. Jewell, K. W. Kemper, D. J. Morrissey, M. Steiner, P. Thirolf, and M. Thoennessen, New region of deformation: The neutron-rich sulfur isotopes, Phys. Rev. Lett. 77, 3967 (1996).
- [15] J. H. Kelley, T. Suomijärvi, S. E. Hirzebruch, A. Azhari, D. Bazin, Y. Blumenfeld, J. A. Brown, P. D. Cottle, S. Danczyk, M. Fauerbach, T. Glasmacher, J. K. Jewell, K. W. Kemper, F. Maréchal, D. J. Morrissey, S. Ottini, J. A. Scarpaci, and P. Thirolf, Proton scattering on the unstable 38 S nucleus: Isovector contribution to the 2_1^+ state, Phys. Rev. C 56, R1206 (1997).
- T. Suomijarvi, J. Kelley, S. Hirzebruch, A. Azhari, D. Bazin, Y. Blumenfeld, J. Brown, P. Cottle, S. Danczyk, M. Fauerbach, T. Glasmacher, J. Jewell, K. Kemper, F. Marechal, D. Morrissey, S. Ottini, J. Scarpaci, and P. Thirolf, Nucl. Phys. A 616, 295
- [17] A. E. Stuchbery, A. D. Davies, P. F. Mantica, P. M. Davidson, A. N. Wilson, A. Becerril, B. A. Brown, C. M. Campbell, J. M. Cook, D. C. Dinca, A. Gade, S. N. Liddick, T. J. Mertzimekis, W. F. Mueller, J. R. Terry, B. E. Tomlin, K. Yoneda, and H. Zwahlen, Shell structure underlying the evolution of quadrupole collectivity in ³⁸S and ⁴⁰S probed by transient-field g-factor measurements on fast radioactive beams, Phys. Rev. C 74, 054307 (2006).
- Davidson, A. N. Wilson, A. Becerril, B. A. Brown, C. M. Campbell, J. M. Cook, D. C. Dinca, A. Gade, S. N. Liddick, T. J. Mertzimekis, W. F. Mueller, J. R. Terry, B. E. Tomlin, K. Yoneda, and H. Zwahlen, Probing shell structure and shape changes in neutron-rich sulfur isotopes through transient-field g-factor measurements on fast ra-

- dioactive beams of ³⁸S and ⁴⁰S., Phys. Rev. Lett. **96**, 112503 (2006).
- [19] H. Otsu, T. Kobayashi, Y. Matsuda, M. Kitayama, K. Inafuku, A. Ozawa, Y. Satou, T. Suda, K. Yoshida, and 1100 H. Sakaguchi, Measurement of the h(38s,p') reaction at 1165 forward angles including 0 degree, Nucl. Phys. A 788. 266 (2007), proceedings of the 2nd International Conference on Collective Motion in Nuclei under Extreme Conditions.
 - B. Longfellow, D. Weisshaar, A. Gade, B. A. Brown, 1170 D. Bazin, K. W. Brown, B. Elman, J. Pereira, D. Rhodes, and M. Spieker, Phys. Rev. C 103, 054309 (2021).
- R. Bansal and J. French, Even-parity-hole states in 7/2shell nuclei, Phys. Lett. 11, 145 (1964). 1110
 - [22] C. Van Der Poel, G. Engelbertink, H. Aarts, D. Scher- 1175 [34] penzeel, H. Arciszewski, and B. Metsch, High-spin states in 34ci, Nucl. Phys. A 373, 81 (1982).
 - [23] C. Van Der Poel, G. Engelbertink, H. Arciszewski, P. Crouzen, J. De Vries, E. Offermann, and E. Evers, High-spin states in 38k, Nucl. Phys. A 394, 501 (1983). 1180
 - [24] E. K. Warburton, D. E. Alburger, J. A. Becker, B. A. Brown, and S. Raman, Probe of the shell crossing at a=40 via beta decay: Experiment and theory, Phys. Rev. C 34, 1031 (1986).
 - [25] Y. Utsuno, T. Otsuka, T. Mizusaki, and M. Honma, Ex-1185 treme location of f drip line and disappearance of the n = 20 magic structure, Phys. Rev. C **64**, 011301 (2001).
- [26] S. Nummela, P. Baumann, E. Caurier, P. Dessagne, A. Jokinen, A. Knipper, G. Le Scornet, C. Miehé, F. Nowacki, M. Oinonen, Z. Radivojevic, M. Ramdhane, 1190 [38] G. Walter, and J. Äystö, Spectroscopy of $^{34,35}\mathrm{Si}$ by β decay: sd - fp shell gap and single-particle states, Phys. Rev. C **63**, 044316 (2001).
- 1130 [27] F. Nowacki and A. Poves. New effective interaction for $0\hbar\omega$ shell-model calculations in the sd-pf valence space, 1195 [39] R. S. Lubna, V. Tripathi, S. L. Tabor, P.-L. Tai, K. Krav-Phys. Rev. C 79, 014310 (2009).
- [28] R. S. Lubna, K. Kravvaris, S. L. Tabor, V. Tripathi, E. Rubino, and A. Volya, Evolution of the n=20 and 28 shell gaps and two-particle-two-hole states in the fsu 1135 interaction, Phys. Rev. Research 2, 043342 (2020).
 - S. Paschalis, I. Lee, A. Macchiavelli, C. Campbell, M. Cromaz, S. Gros, J. Pavan, J. Qian, R. Clark, H. Crawford, D. Doering, P. Fallon, C. Lionberger, T. Loew, M. Petri, T. Stezelberger, S. Zimmermann, D. Radford, K. Lagergren, D. Weisshaar, R. Winkler, 1205 T. Glasmacher, J. Anderson, and C. Beausang, The performance of the gamma-ray energy tracking in-beam nuclear array gretina, Nucl. Instrum. Meth. A 709, 44 (2013).

1140

1150

1155

- [30] C. Davids, B. Back, K. Bindra, D. Henderson, 1210 [41] P. T. MacGregor, D. K. Sharp, S. J. Freeman, C. R. Hoff-W. Kutschera, T. Lauritsen, Y. Nagame, P. Sugathan, A. Ramayya, and W. Walters, Startup of the fragment mass analyzer at atlas, Nucl. Instrum. Meth. B 70, 358 (1992).
- [31] S. J. Freeman, R. V. F. Janssens, B. A. Brown, M. P. 1215 Carpenter, S. M. Fischer, N. J. Hammond, M. Honma, T. Lauritsen, C. J. Lister, T. L. Khoo, G. Mukherjee, D. Seweryniak, J. F. Smith, B. J. Varley, M. Whitehead, and S. Zhu, Low-lying levels in ⁵⁹Cr: Inadequacy of the fp model space and onset of deformation, Phys. Rev. C 1220 **69**, 064301 (2004).
- S. Zhu, A. N. Deacon, S. J. Freeman, R. V. F. Janssens, B. Fornal, M. Honma, F. R. Xu, R. Broda, I. R. Calderin, M. P. Carpenter, P. Chowdhury, F. G. Kondev, 1160

- W. Królas, T. Lauritsen, S. N. Liddick, C. J. Lister, P. F. Mantica, T. Pawłat, D. Seweryniak, J. F. Smith, S. L. Tabor, B. E. Tomlin, B. J. Varley, and J. Wrzesiński, Level structure of the neutron-rich $^{56,58,60}\mathrm{Cr}$ isotopes: Singleparticle and collective aspects, Phys. Rev. C 74, 064315 (2006).
- [33] A. N. Deacon, J. F. Smith, S. J. Freeman, R. V. F. Janssens, M. P. Carpenter, B. Hadinia, C. R. Hoffman, B. P. Kay, T. Lauritsen, C. J. Lister, D. O'Donnell, J. Ollier, T. Otsuka, D. Seweryniak, K.-M. Spohr, D. Steppenbeck, S. L. Tabor, V. Tripathi, Y. Utsuno, P. T. Wady, and S. Zhu, Cross-shell excitations near the "island of inversion": Structure of ³⁰Mg, Phys. Rev. C **82**, 034305 (2010).
- A. Boehnlein, M. Diefenthaler, C. Fanelli, M. Hjorth-Jensen, T. Horn, M. P. Kuchera, D. Lee, W. Nazarewicz, K. Orginos, P. Ostroumov, L.-G. Pang, A. Poon, N. Sato, M. Schram, A. Scheinker, M. S. Smith, X.-N. Wang, and V. Ziegler, Artificial intelligence and machine learning in nuclear physics (2021), arXiv:2112.02309 [nucl-th].
- [35] K. He, X. Zhang, S. Ren, and J. Sun, Delving deep into rectifiers: Surpassing human-level performance on imagenet classification (2015), arXiv:1502.01852 [cs.CV].
- [36] N. Srivastava, G. Hinton, A. Krizhevsky, I. Sutskever, and R. Salakhutdinov, Dropout: A simple way to prevent neural networks from overfitting, J. Mach. Learn. Res. **15**, 1929–1958 (2014).
- [37] D. P. Kingma and J. Ba, Adam: A method for stochastic optimization (2017), arXiv:1412.6980 [cs.LG].
- R. S. Lubna, K. Kravvaris, S. L. Tabor, V. Tripathi, A. Volya, E. Rubino, J. M. Allmond, B. Abromeit, L. T. Baby, and T. C. Hensley, Structure of ³⁸Cl and the quest for a comprehensive shell model interaction, Phys. Rev. C **100**, 034308 (2019).
- varis, P. C. Bender, A. Volya, M. Bouhelal, C. J. Chiara, M. P. Carpenter, R. V. F. Janssens, T. Lauritsen, E. A. McCutchan, S. Zhu, R. M. Clark, P. Fallon, A. O. Macchiavelli, S. Paschalis, M. Petri, W. Reviol, and D. G. Sarantites, Intruder configurations of excited states in the neutron-rich isotopes ³³P and ³⁴P, Phys. Rev. C 97, 044312 (2018).

1200

- [40] D. Chrisman, A. N. Kuchera, T. Baumann, A. Blake, B. A. Brown, J. Brown, C. Cochran, P. A. DeYoung, J. E. Finck, N. Frank, P. Guèye, H. Karrick, H. Liu, J. McDonaugh, T. Mix, B. Monteagudo, T. H. Redpath, W. F. Rogers, R. Seaton-Todd, A. Spyrou, K. Stiefel, M. Thoennessen, J. A. Tostevin, and D. Votaw, Phys. Rev. C **104**, 034313 (2021).
- man, B. P. Kay, T. L. Tang, L. P. Gaffney, E. F. Baader, M. J. G. Borge, P. A. Butler, W. N. Catford, B. D. Cropper, G. de Angelis, J. Konki, T. Kröll, M. Labiche, I. H. Lazarus, R. S. Lubna, I. Martel, D. G. McNeel, R. D. Page, O. Poleshchuk, R. Raabe, F. Recchia, and J. Yang, Phys. Rev. C **104**, L051301 (2021).
- [42] J. Williams, G. C. Ball, A. Chester, P. Choudhary, T. Domingo, A. B. Garnsworthy, G. Hackman, J. Henderson, R. Henderson, R. Krücken, R. S. Lubna, J. Measures, O. Paetkau, J. Park, J. Smallcombe, P. C. Srivastava, K. Starosta, C. E. Svensson, K. Whitmore, and M. Williams, Phys. Rev. C 102, 064302 (2020).
- [43] B. Abromeit, S. L. Tabor, V. Tripathi, R. S. Lubna, D. Caussyn, R. Dungan, K. Kravvaris, E. Rubino, P.-

L. Tai, and A. Volya, Phys. Rev. C 100, 014310 (2019).